M.H


*Institute of Paper Science and Technology*
*Atlanta, Georgia*

**IPST TECHNICAL PAPER SERIES**

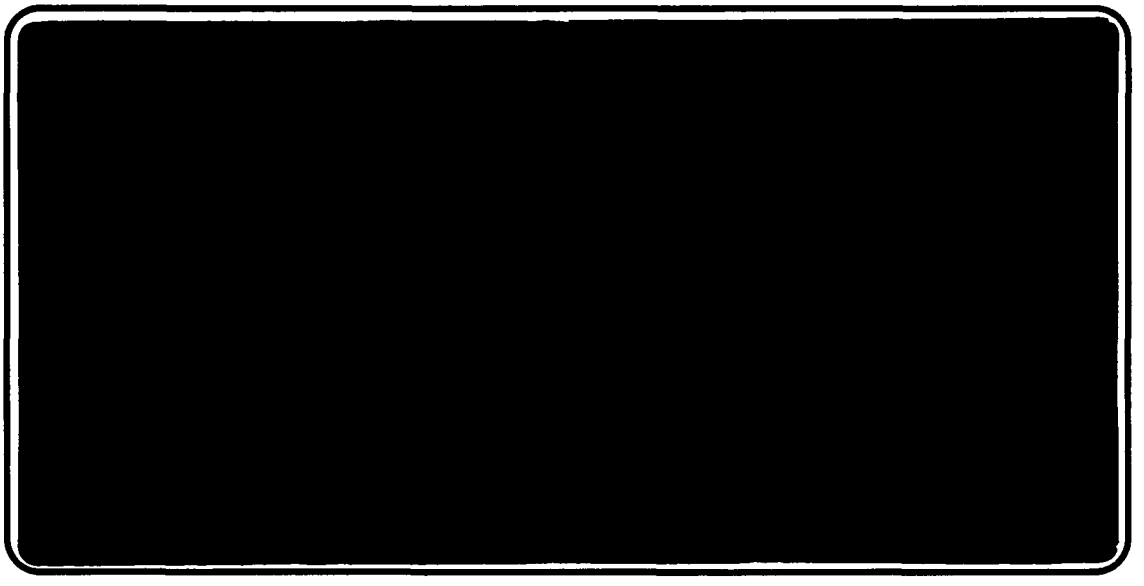

NUMBER 369

# FLUID DYNAMICS OF SHORT-DWELL COATER PONDS AND THEIR RELATIONSHIP TO COAT WEIGHT NONUNIFORMITIES

N.G. TRIANTAFILLOPOULOS AND C.K. AIDUN

DECEMBER, 1990

# Fluid Dynamics of Short-Dwell Coater Ponds and Their Relationship to Coat Weight Nonuniformities

N.G. Triantafillopoulos and C.K. Aidun

Winner of the 1990 George Olmsted Award
American Paper Institute

# FLUID DYNAMICS OF SHORT-DWELL COATER PONDS AND THEIR RELATIONSHIP TO COAT WEIGHT NONUNIFORMITIES

Nicholas G. Triantafillopoulos and Cyrus K. Aidun
Graduate Student and Assistant Professor
The Institute of Paper Science and Technology
Atlanta, Georgia

## ABSTRACT

Short-dwell blade coaters have efficiently increased productivity and imparted desired sheet properties, especially for lightweight coated grades. However, the trend to increase machine speed while reducing coat weight has been hindered by the difficulty of attaining uniform coat weight profiles, particularly when applying formulations containing delaminated clays. Although CD metering variations have limited the maximum machine speed in a number of applications (e.g., short-dwell coaters, size presses, flexographic printers, etc.), it appears that no published studies show the cause of this problem. Using experimental flow visualization techniques, pilot scale trials, and computational fluid dynamics analysis, we show that the problems originate from the three-dimensional instabilities developing in the pond upstream of the blade. Such flows determine the transport phenomena which influence the mass and momentum transfer into the metering zone and, hence, are indirectly responsible for film thickness nonuniformities.

In this paper, we examine the connection between expected flows in short-dwell ponds and the "streaky" appearance of lightweight coated paper. The specific objectives were (a) to characterize the flow in a geometry similar to short-dwell ponds as the machine speed changes, and (b) to systematically document the onset and appearance of streaks with pilot plant trials. Flow visualization studies were conducted with both a Newtonian fluid and a typical shear-thinning coating color using optical and novel flash x-ray techniques.

The short-dwell pond was experimentally simulated as a lid-driven cavity, i.e., a rectangular box wherein the flow is induced by the movement of the top boundary, with through flow. Flow visualization studies revealed multiple steady states and successive states of unstable three-dimensional flows as the characteristic Reynolds number, based on lid velocity and cavity width, increased. Centrifugal instabili-

ties induce formation of three-dimensional Taylor-Görtler-like vortices which drive the hydrodynamic system sequentially to time-periodic motion, violently fluctuating, and eventually chaotic flows. Flash x-ray studies show for the first time that similar structures exist at a certain Reynolds number with both the Newtonian and coating fluids. Appearance of three-dimensional flows is in agreement with numerical simulations of two-dimensional ponds which unveiled the existence of two counter-rotating vortices with strong centrifugal forces, a sufficient requirement for onset of three-dimensional instabilities. In addition, nonlinear dynamical analysis proves the possibility of multi-stable states observed in the flow visualization experiments. The existence of multiple stable states of flow at the same machine speed explains the past difficulties in predicting the system behavior.

Within the range of shear viscosity for the high-viscosity colors investigated, appearance of streaks on lightweight coated papers correlates with expected onset of hydrodynamic instabilities in the pond and violent fluctuations of the flow in the cross machine direction. For a pilot coater having a span-to-width ratio of 10:1, streaks appear in their marginal form for a Reynolds number (based on machine speed, Brookfield viscosity and coater pond width) in the range from 550 to 750, and in their severe form for values greater than 1100. These results, obtained with viscosity of at least 900 mPa.s, suggest that pond hydrodynamics are indirectly responsible for the streaks. We show that, in general, hydrodynamic instability in the pond constitutes a sufficient but not necessary condition for development of a nonuniform profile.

**Keywords:** Blade Coater, Short-dwell Coater, Fluid Dynamics, Instabilities, Coatability, CD profile, Rheology

## INTRODUCTION

Blade coaters are the most common method for high-speed coating of paper and paperboard. Production efficiency in online coating operations, the method of choice in the U.S., is dependent on the ability of the coater to run at high speeds while consistently delivering a product of uniform quality in both the machine-, and cross-machine directions. As paper machine speeds push new limits, it is essential

to design compatible coating systems. Similar requirements also apply to other systems for surface treatment of paper webs such as modern size presses.

Blade coaters and size presses with short-dwell-time applicators have gained popularity over the past ten years due to their compactness, operational efficiency, and increased productivity. In contrast to systems with an applicator roll, color penetration into the sheet prior to metering is minimal and, all other parameters remaining constant, a certain coat weight can be attained with lower blade pressure. Thus, not only are paper strength properties retained, but web breaks are reduced and productivity increases.

The trend toward increasing machine speed while reducing coat weight in bevelled blade operations with a short-dwell coater (SDC) has been hindered by difficulty in maintaining uniform cross directional (CD) coat weight profile, especially in the production of light weight coated (LWC) papers. Spatially and temporally periodic, sometimes even random, coating thickness variations create an uneven CD profile which, in its extreme case, appears as streaks running along the machine direction. Wet streaks several centimeters in width, also called patches, comprise areas of comparatively low film thickness which are independent of base stock formation characteristics and the microroughness of paper (Fig. 1). This macroscale streaking pattern is visually more profound at machine speeds above 1000 m/min when using formulations with a large portion of delaminated clays; pigments desirable for their print quality but whose runnability is not conducive to high machine speeds and solids content. Consequently, there seems to be a coatability limit with SDC. That is, for a given set of operating conditions and fluid shear-viscosity, a maximum coating speed exists above which, for a slight increase in machine speed, the CD coat weight profile is uncontrollable, i.e., with variations beyond statistically acceptable and controllable levels. In addition, the system is unpredictable because "disturbances" can irreversibly change operational characteristics and, therefore, influence product quality and its uniformity.

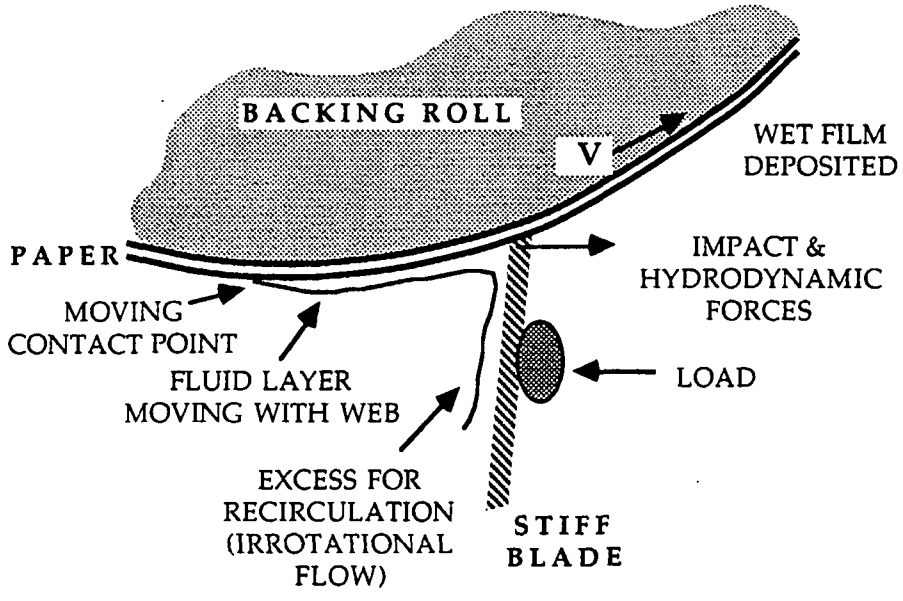


**Figure 1.** Schematic illustration of the bevelled-blade coating process in a short-dwell coater (not in scale).

Motivated by the need to unveil a possible origin of the coat weight nonuniformities, a fundamental study is undertaken to systematically investigate the fluid dynamics in SDC ponds. In particular, it is shown that three-dimensional hydrodynamic instabilities inside the pond are indirectly responsible for, and hence correlate with, wet-film thickness variations across the machine direction. The relevant argument is that pond flows manifest the transport phenomena which influence the mass and momentum transfer into the blade nip and, consequently, affect coat weight and its uniformity. Central to this approach is the thickness and uniformity (along the span of the doctoring blade) of the coating color layer traveling with the moving web which is eventually delivered into the blade nip (Fig. 2).

In systems with an applicator roll and absence of film splitting at the application nip, this layer is well-defined. A fundamental difference exists between the characteristics of the layer entering the blade nip of a SDC compared to the nearly irrotational layer (1) in a system with a roll applicator. In the case of a SDC, a viscous layer forms near the dynamic contact line, upstream of the blade nip. This layer is susceptible to instability, and interaction with the dynamic contact line or the three-dimensional patterns of flow develop as the nearly irrotational eddies inside the SDC pond destabilize. These interactions,

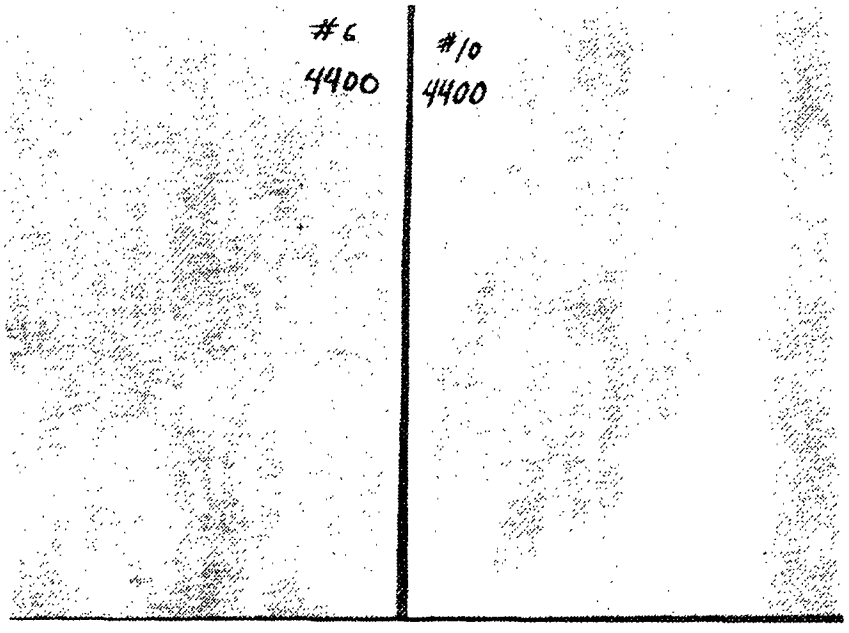


Figure 2. Photographs illustrating the streaky appearance of LWC. papers coated in the pilot plant at 1340 m/min (4400 fpm).

which generate a nonuniform wavy layer entering the blade nip, could adversely affect the uniformity of the coat weight profile.

The isothermal confined flow in SDC ponds, like the flow in a lid-driven rectangular cavity, is driven by the shear stress imposed on the fluid by the moving web. Eklund, et al., demonstrated with flow visualization experiments (2) and limited numerical simulations (3) that two-dimensional recirculating vortices prevail inside the pond. These authors also suggest that centrifugal forces of the two-dimensional recirculating vortices may generate viscosity stratification by inducing localized concentration gradients of pigment particles. The concentration gradient referred to by these authors, however, is in a plane parallel to the machine-line direction. This alone cannot generate coat weight nonuniformities in the CD, the topic which is of primary concern in this study. Other more elaborate computer models (4-6) verify, at least qualitatively, the visualization results and give better insight into the flow phenomena involved. Although all of the computer models of SDC pond flows consider only the two-dimensional equations and therefore cannot predict three-dimensional phenomena, they confirm the existence of strong recirculating eddies which are susceptible to three-dimensional instabilities. It is well-established that curvilinear streamlines are susceptible to centrifugal hydrodynamic instabilities with three-dimensional cellular structures and eventually chaotic behavior (7). Thus, a question that remains unanswered is how and to what degree does the transition from two- to three-dimensional flows in SDC ponds influence the uniformity of the coat weight profile.

Although "turbulence" in the SDC pond has been proposed by many authors (8-14) as the possible cause for coat weight profile nonuniformity, there is no published experimental data or other systematically documented evidence to support this argument. Furthermore, as will be shown below, turbulent flow is found to start at machine speeds in excess of the current operating limits.

Not only is it possible for various forms of hydrodynamic instabilities to set in, but the system may also have multiple stable states due to edge effects. Such effects can induce three-dimensional cellular structures in the pond, which eventually convect into the blade nip and may cause coat weight variations. Revealing the rich nature and forms of these flows contributes to appreciation of the differences observed in practice between systems with an applicator roll and short-dwell coaters. Furthermore, it is desirable

to study the characteristic flows in SDC ponds, which are virtually unexplored, in order to predict machine runnability. This knowledge will lead to better control of the process and expansion of its operating window. Ultimately, information on the fluid flow aspects of the system would provide the basis for the design of future generations of coaters.

The systematic program of research implemented to investigate the fluid dynamics in SDC ponds consisted of four parts: (a) laboratory flow visualization experiments were conducted in a geometry similar to a short-dwell pond, (b) the two-dimensional flow in SDC ponds was numerically simulated, (c) pilot-plant trials were conducted in an attempt to correlate the expected flow in the pond with the appearance of wet streaks on paper, and (d) analysis based on nonlinear dynamics assisted in interpreting the results and explaining how the observed states of flow can exist.

Although small portions of the experimental (15) and numerical results (4,5) have been published before, this paper is the first comprehensive presentation of the findings from this study. The experimental work reveals the rich nature of flow structures in SDC ponds as the speed of the machine increases. It also illustrates that the hydrodynamic system may operate under competing operating states. Then, it presents the connection between the hydrodynamics inside the pond with the appearance of visible wet streaks on the coated web.

Flow visualization experiments are performed with a Newtonian fluid (i.e., glycerol) and a coating color using the aluminum-flake, direct dye-injection, and flash x-ray radiographic techniques. The latter allow for the first time, to visualize the flow through opaque coating colors. This study focus on qualitative features of the fully developed flow observed as the speed which drives the flow progressively changes. Pilot coater trials are based on a typical coating formulation for rotogravure which has illustrated "problematic" runnability, i.e., formulations containing delaminated clays and having comparatively high Brookfield shear-viscosity.

The main body of the paper is divided into four parts. The first part describes qualitative flow phenomena from the laboratory facility after providing a background description of methods and techniques used. The second part reviews briefly the findings from computational experiments of the two-dimensional flow performed on a computer. The third part contains background information and presents the results

from pilot-plant trials. The fourth part presents an analysis based on theory which supports the experimental findings. A separate section included at the end discusses the impact of the results from this work.

## LABORATORY EXPERIMENTS

### BACKGROUND

The flow in short-dwell coater ponds has been simulated experimentally as a shear-driven flow in a rectangular cavity with finite spanwise length (Fig. 3). Furthermore, to incorporate the essence of relevant physics, a relatively small flux of fluid was allowed to pass through the cavity. Enclosed lid-driven cavities constitute a relatively simple geometry to study recirculating flows in fluid dynamics and have been used extensively, at least in their two-dimensional form, in benchmark problems to test numerical codes. Their flow is characterized by a Reynolds number, Re, defined as:

$$\mathrm{Re} = \frac{\rho V D}{\mu},$$

where V is the velocity of the lid which induces the flow, D is the width of the cavity, and $\mu$ and $\rho$ are the viscosity and density of the fluid, respectively. For cavities with through-flow, however, an additional dimensionless parameter is required to uniquely define the flow. This is the Reynolds number ($Re^*$) based on the net mass flow rate, m, per unit span length and time passing through the cavity, and the spanwise (along the CD) aspect ratio, S:

$$\mathrm{Re}^* = \frac{m}{\mu S}.$$

Flow visualization experiments performed during the course of this study were for Re between 100 and 9000, while the range for $Re^*$ varied from 0.10 to 0.80. Within this range, the through-flow cavity has flow characteristics similar to a nearly enclosed lid-driven cavity ($Re^*<0.01$).

The enclosed lid-driven cavity flow has been studied extensively both experimentally and computationally. A comprehensive review of the literature is included elsewhere (16). Here we highlight key characteristics of the flow, as determined from previous experimental work, which has relevance to the visualization experiments performed during the course of our work.

The two-dimensional flow depicted in Fig. 4 represents the basic stable state of the system. The primary recirculating vortex (a roll in three dimensions) drags fluid from the top lip of the cavity, E, down along the vertical downstream wall, EF. However, at some distance along the wall the moving fluid can no longer sustain frictional forces and separation occurs, thus forming the downstream secondary vortex (DSV). Similarly, secondary vortices appear at the lower and upper corners of the upstream vertical wall, AG. These are weaker flows than the primary roll but, as will be seen later, they have substantial impact on the flow. In general, these vortical structures have also been resolved by numerical simulations.

The most recent experimental studies of lid-driven cavities are by Koseff (16), Koseff and Street (17), and Prasad and Koseff (18). They used an impulsively-started lid to approach specific Reynolds numbers, Re, between 1000 and 10,000. The main conclusions of their work are: (a) the flow is three-dimensional for Re greater than 1000, exhibiting Taylor-type centrifugal instabilities during startup and Taylor-Görtler-like (TGL) vortices when fully developed, (b) end-wall effects influence the flow by inducing three-dimensionality, and (c) turbulence occurs for Re above 6000. Most of the activity takes place in the vicinity of the DSV, which led Koseff and Street (17) to suggest that these centrifugal instabilities arise from destabilization of the boundary layer between the primary and the secondary rolls.

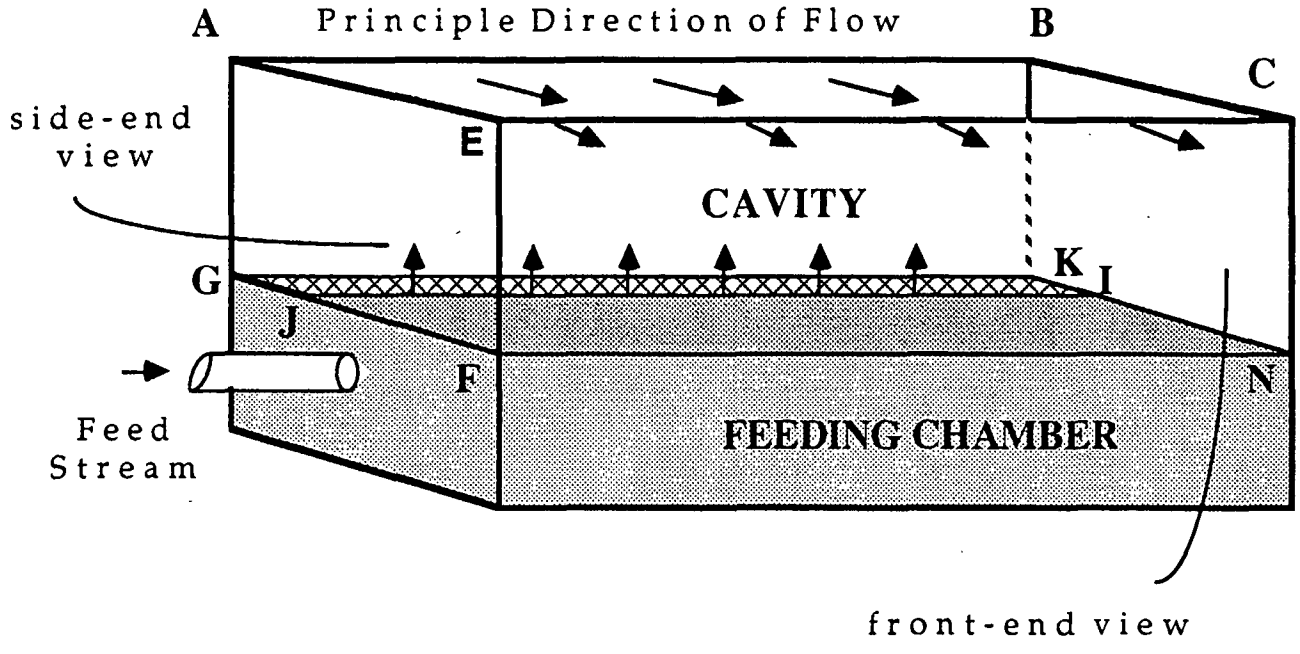


Figure 3. Schematic drawing of a lid-driven cavity with through-flow used in the experiments of this study (not in scale).

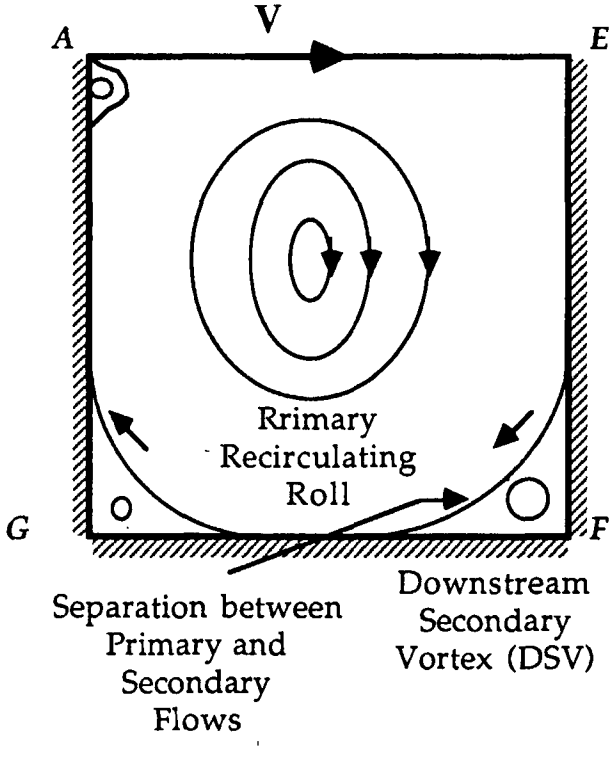


Figure 4. Illustration of the two-dimensional flow in a lid-driven cavity.

It is worth emphasizing that existence of these vortices does not indicate turbulent flow, which was reported to appear only for Re between 6000 and 8000 (16). However, the transitional mode of these evolving structures as a function of Re was not studied. Also, the rich and interesting features of flow at Re smaller than 1000, where most coating systems operate due to the highly viscous nature of coating colors, has remained unexplored. Two fundamental questions which remain unanswered are (a) what is the route the system takes to turbulence, and (b) is this route unique or are there alternative sequences of transitions from laminar to turbulent flow.

## EXPERIMENTAL SETUP

In the context described above and considering actual practices in short-dwell coating operations, key to simulating the pond flow is dynamic similarity between the experimental cavities and SDC ponds. This can be achieved by matching the two dimensionless numbers, Re and Re*. In this study the geometric scales of the cavity with respect to depth (D) and width (H) are identical with D=H=1, and the physical dimension is 5.08 cm (width in the case of SDC ponds is considered the distance between the bevel of the blade and the overflow baffle). The span of the cavity used is 15.24 cm, which gives a spanwise aspect ratio S/H equal to 3. Admittedly, this is much smaller than the spanwise aspect ratio of the actual short-dwell coaters, which varies between 100 and 200 depending on the width of the machine. So, the experimental results are mainly qualitative. The Reynolds number Re in SDC ponds can attain values from several hundreds to a few thousands depending on speed and color viscosity [e.g., Re equals 1400 for 1200 m/min (about 4000 fpm) machine speed, blade-to-baffle distance of 5.00 cm, $\rho$=1.40 g/cc, and $\mu$=1000 mPa.s]. The value of simple shear viscosity (called viscosity hereafter) chosen for the calculations is based on a measurement with a Brookfield viscometer at 100 rpm (spindle no. 3) - a valid quantity considering that the bulk of the fluid inside a pond experiences relatively low shear rates of the order of magnitude of a few hundred reciprocal seconds. In the case of coating colors, viscosity is shear- and time-

dependent. Only an "apparent" Reynolds number can be calculated based on this type of a single-point viscometric measurement.

The Reynolds number Re* is proportional to the pumping rate, which typically varies between 4 and 14 $m^3/hr$. The dimensionless parameters of the cavity were altered by changing first the peripheral speed of the roll, V, and then the fluid viscosity, $\mu$, and feeding flow rate. However, the range over which fluid properties and experimental operating conditions were free to vary were limited by practical considerations.

The principal component of the experimental setup is the cavity area of interest (Fig. 3) upon which a rotating cylindrical roll supplying the driving force rests. The cavities have been manufactured from Plexiglas for easy visualization. The lower compartment comprises the feeding chamber through which fluid enters the cavity area via a 1-cm wide perforated plate (3.2 mm holes, 40% open) next to the upstream vertical wall, ABKG. A 1.0 cm thick Teflon® collar around the cavity lip, ABCE, allows for smooth contact with the roll surface. A thin film is deposited onto the roll and exits the cavity from edge EC, very much like the physical arrangement in a bevelled blade SDC. Because the interest here is the flow phenomena in the cavity, no overflow was allowed for, thus minimizing the influence of a moving contact line upstream. Air inclusion in the cavity may occur as the peripheral roll speed increases, but it can be avoided by properly adjusting the feeding flow rate and the hydraulic pressure that keeps the cavity in contact with the roll. More details on the experimental facility and its operation are included elsewhere (19).

In most of the visualization experiments, we used various mixtures of glycerine in water having viscosity between 77 and 160 ± 3 mPa.s (Brookfield viscometer, spindle no. 3, 100 rpm) and density of 1.26 to 1.28 ± 0.04 g/cc. A limited number of visualization experiments were conducted with a sodium alginate solution ($\mu$=95 mPa.s and $\rho$=1.1 g/cc). The preferred method for visualization was the suspended-particles technique (20) where disk-shaped, high reflectance aluminum flakes (340 mesh) are suspended in the fluid continuum at concentrations of up to 0.1% by weight. These flakes act as neutrally buoyant markers and can provide photographic images of the instantaneous state of flow, or the evolution of periodic and unsteady states on a videotape. In addition, direct-dye injection techniques (21) were also used to

indirectly reveal the accumulated results of transport processes occurring in the cavity. This technique can unveil the form of flow structures. Some qualitative data were obtained with typical coating colors at 60% solids content by using the novel flash x-ray radiographic (FXR) technique described in a previous paper (22). The tracer here was a CMC solution containing approximately 50% by weight sodium tungstate, a substance which has one of the highest mass x-ray absorption coefficients. The density and viscosity of this fluid were similar to the coating color.

## FLOW VISUALIZATION RESULTS

In a laboratory, we evaluated phenomena appearing in driven cavity flows with through-flow using real-time observation and photographs of flow patterns. The flow in the cavity is changed by increasing the roll speed in increments. The photographs presented here depict the front-end view of a cavity as a spanwise plane parallel to downstream wall EFCN in Fig. 3. Limited observations from a side-end view parallel to end-wall AEFG reveal the basic flow characteristics illustrated in Fig. 4, thus confirming the similarity of the flow considered here and the enclosed lid-driven flow. However, the interest concentrates on the three-dimensional flow structures along the spanwise direction of the cavity (the CD of the machine).

The control parameter that describes the flow is the cavity Reynolds number, Re, as estimated from repeated flow visualization experiments. Gradual increase of the peripheral roll speed takes the system from its two-dimensional, steady state (the base stable state) to time-periodic and unsteady states featuring three-dimensional cellular structures. Toroidal eddies in the form of Taylor-Görtler-like vortices meander along the spanwise direction of the cavity with their axes parallel to the principal direction of flow. These structures are centrifugal instabilities inherent to system dynamics and are relatively weak at onset but grow in strength with roll speed. Similar structures are obtained during sudden startup of the flow when the value of the Re is above a certain critical range. Table I presents the critical ranges and corresponding observations estimated from flow visualization experiments using square

cavities with spanwise aspect ratio of 3. Following is a brief description of the flow patterns observed with the aluminum-flake technique.

When the cavity Reynolds number remains below approximately 500, the two-dimensional flow is stable and steady, featuring mainly the primary and downstream secondary rolls. A front view of the two rolls appears in Fig. 5. (The dark line is the interface separating the rolls.) For Re in the range of 500 to 600, vertical dark spikes are generated at the centerline and start traveling toward both side end walls (edges). At Re increases up to about 1100, the separation line becomes wavy, and the waves subsequently engage in a complex spanwise oscillatory motion. At this point, spikes grow small crowns at their tops which give them a mushroom-like form (Fig. 5). As the speed slowly increases, the flank and stem of the mushrooms first oscillate in-phase and eventually fluctuate causing the flanks to alternatively jump rapidly from left to right, thus giving the appearance they are disappearing into their neighbors and reappearing a short while later. These phenomena are considered to indicate an unsteady state.

The direct-dye technique gives a better assessment of the kind of structures that superimpose on the base stable state because it represents accumulated results of all transport processes that carry the injected fluid. When the tracing fluid is injected close to edge EC along the flow down the wall EFCN (in Fig. 3) a horseshoe-shaped structure is formed inside the DSV and next to the bottom boundary (Fig. 6). These are very similar to the three-dimensional vortices arising from centrifugal instabilities in enclosed lid-driven cavity flows termed TGL vortices by Koseff (16), and Koseff and Street (17). These vortices appear in pairs along the span of the cavity, so that a horseshoe-shaped structure is riding on a pair of TGL vortices. This feature is illustrated in the shadowgraph, obtained with the FXR technique (Fig. 7) where the bulk fluid is a typical coating color. Such similarities between Newtonian and coating fluids imply that flow features, prevailing above a critical range of the control parameter, exist irrespective of the type of fluid. Thus, the mushroom-like structures appearing with the aluminum-flake technique are present in the cross-section of the vertical interface between two neighboring TGL vortices, as depicted in Fig. 8.

The results presented above demonstrate that the flow in a lid-driven rectangular cavity with small through-flow is susceptible to three-dimensional centrifugal instabilities as the Reynolds number Re increases. These instabilities arise from imbalances induced by competing centrifugal forces (due to

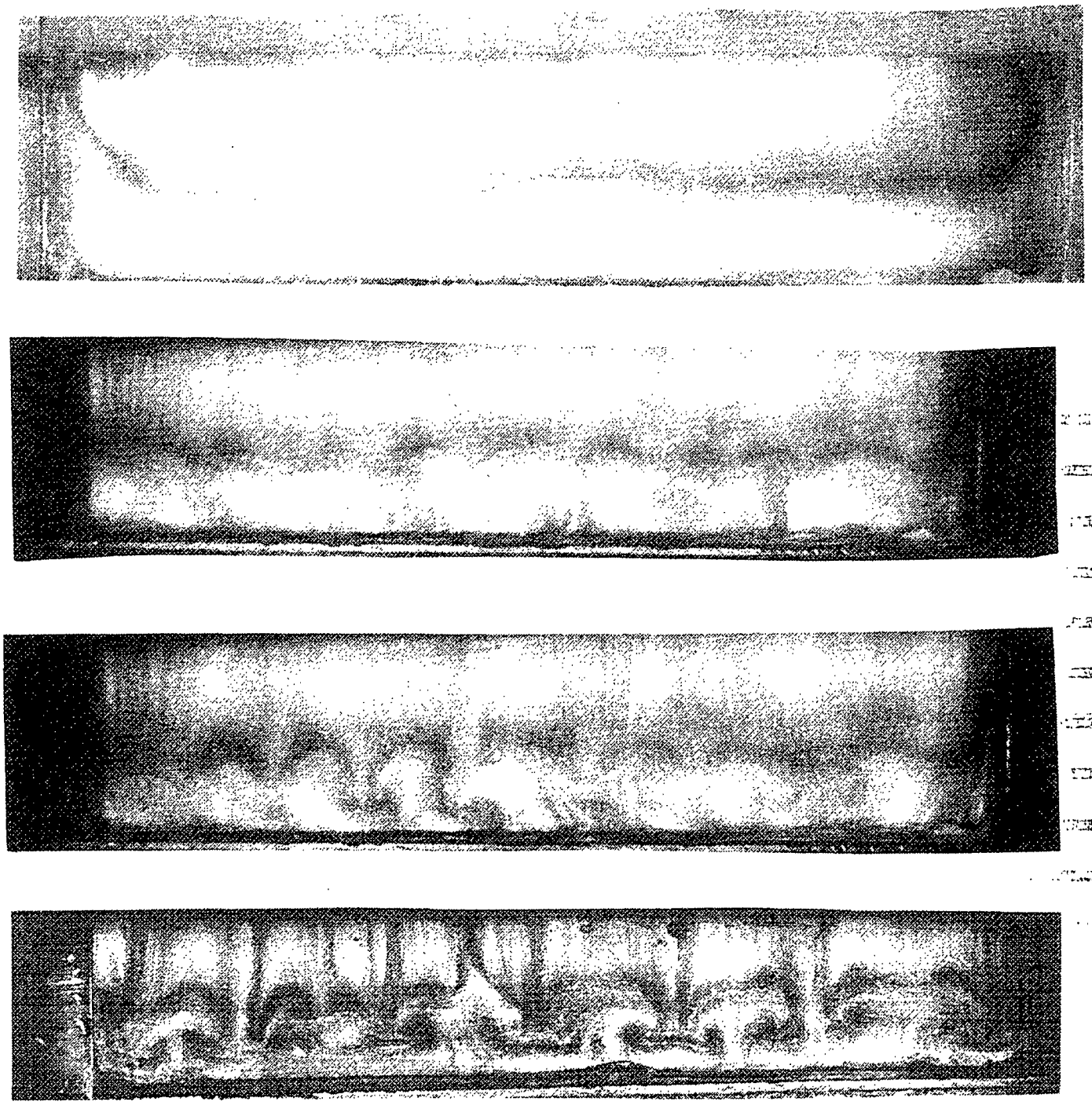


**Figure 5.** Front-view photographs of flow patterns. From top to bottom: (a) two-dimensional steady flow with primary and secondary rolls at Re=500 (notice the straight separation line); (b) wavy separation line for Re=700-1000 (time-periodic flow); (c) appearance of mushroom-like structures for Re=1100; (d) unsteady state at Re=1900.

Figure 6. A direct-injection image of a horseshoe-shaped structure in the vicinity of the DSV near the middle of the cavity (Re=500). This structure is riding on a pair of Taylor-Görtler-like vortices. The bulk fluid is glycerol in water.

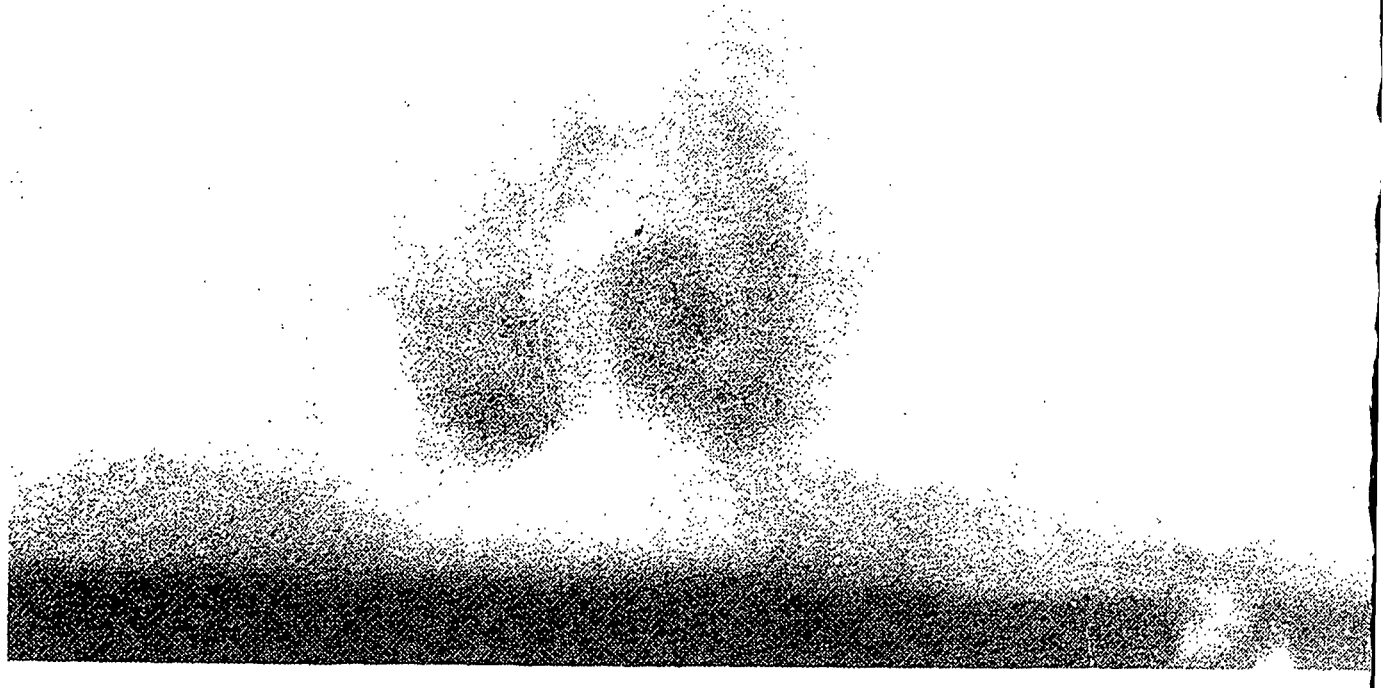

Figure 7. Flash X-ray radiographic image of a pair of Taylor-Görtler-like vortices appearing in the vicinity of the DSV near the middle of the cavity. Re=590, $Re^*$=0.35. The bulk fluid is a typical coating color for rotogravure LWC with 62% solids content. Image magnified to show details.

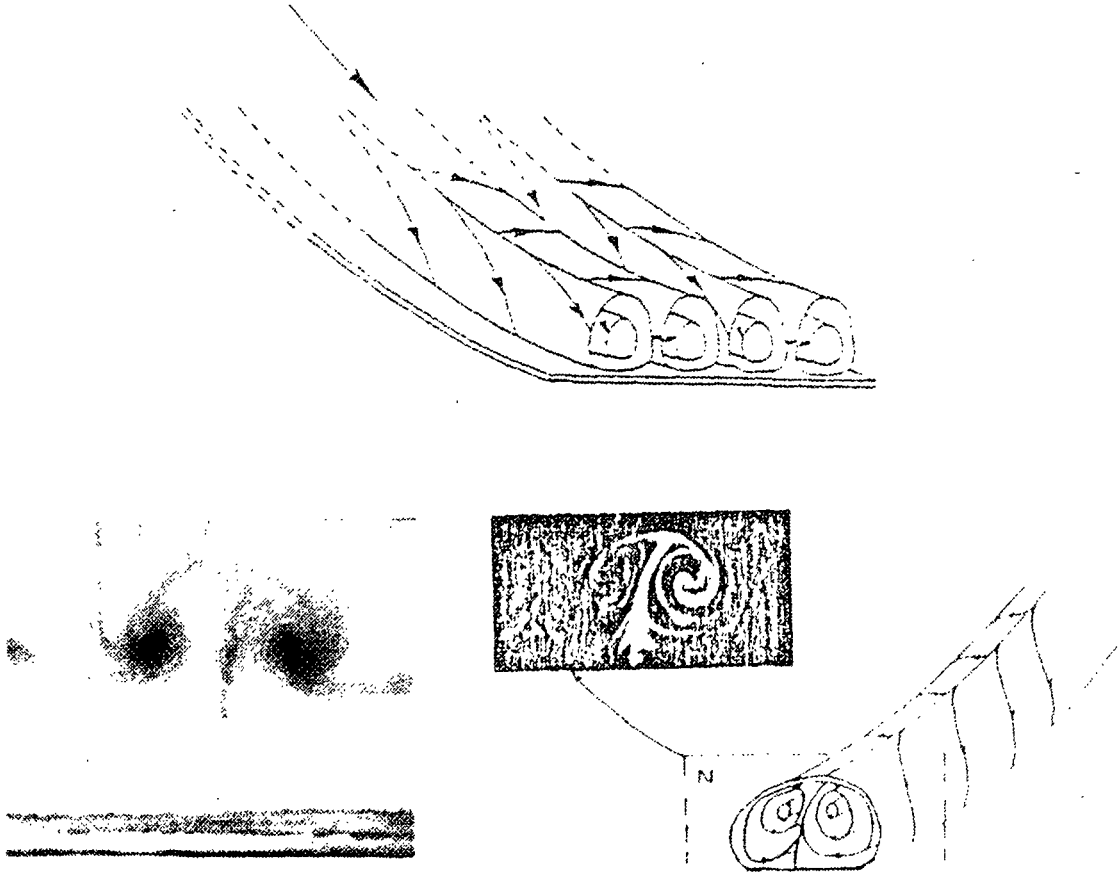

Figure 8. Schematic of Taylor-Görtler vortices as they appear over concave walls. On the left is a photograph of the mushroom-like structure inside the DSV at the middle of the cavity using the aluminum-flake technique. The fluid is glycerol in water.

curvilinear streamlines of recirculating rolls) and the pressure gradient, created in a manner similar to the Taylor vortices appearing in Couette flow (23) and the Görtler vortices appearing in boundary layer flows over concave walls (24). Interestingly, the sequence of evolving structures described above is reminiscent of the instability of a laminar boundary layer flowing over a concave wall (25).

**Table I.** Estimated critical Reynolds numbers from flow visualization experiments (Lid-driven cavity with small through-flow, $Re^*<0.80$, D/H=1:1, S/H=3:1).

| Re | Observations |
|---|---|
| Above 500 | A time-periodic, three-dimensional instability superimposes on the DSV of the basic two-dimensional state. |
| 600-700 | Separation line between the primary recirculation and the DSV becomes wavy; waves travel in spanwise direction starting from the centerline. |
| 900-1000 | Violent spanwise oscillation of waves. |
| 1100 and up | Unsteady mushroom-like structures fluctuate violently inside the DSV. Whole flow regime becomes unstable. |

A more intriguing and potentially useful feature is the appearance of large-scale three-dimensional structures at low to moderate Reynolds numbers which compete with the stable two-dimensional flow. Depending on the procedure followed to attain a certain speed, an array of counter-rotating cellular structures stabilizes and replaces the base state. Three possible patterns are presented in Fig. 9. This is an important piece of information regarding the dynamical behavior of the hydrodynamic system. Although the multiple states of flow are stable to infinitesimal disturbances, they are unstable to finite-amplitude disturbances, i.e., the system is locally stable but globally unstable (7). Physical characteristics and consequences of globally unstable flows in short-dwell coaters are discussed elsewhere (26).

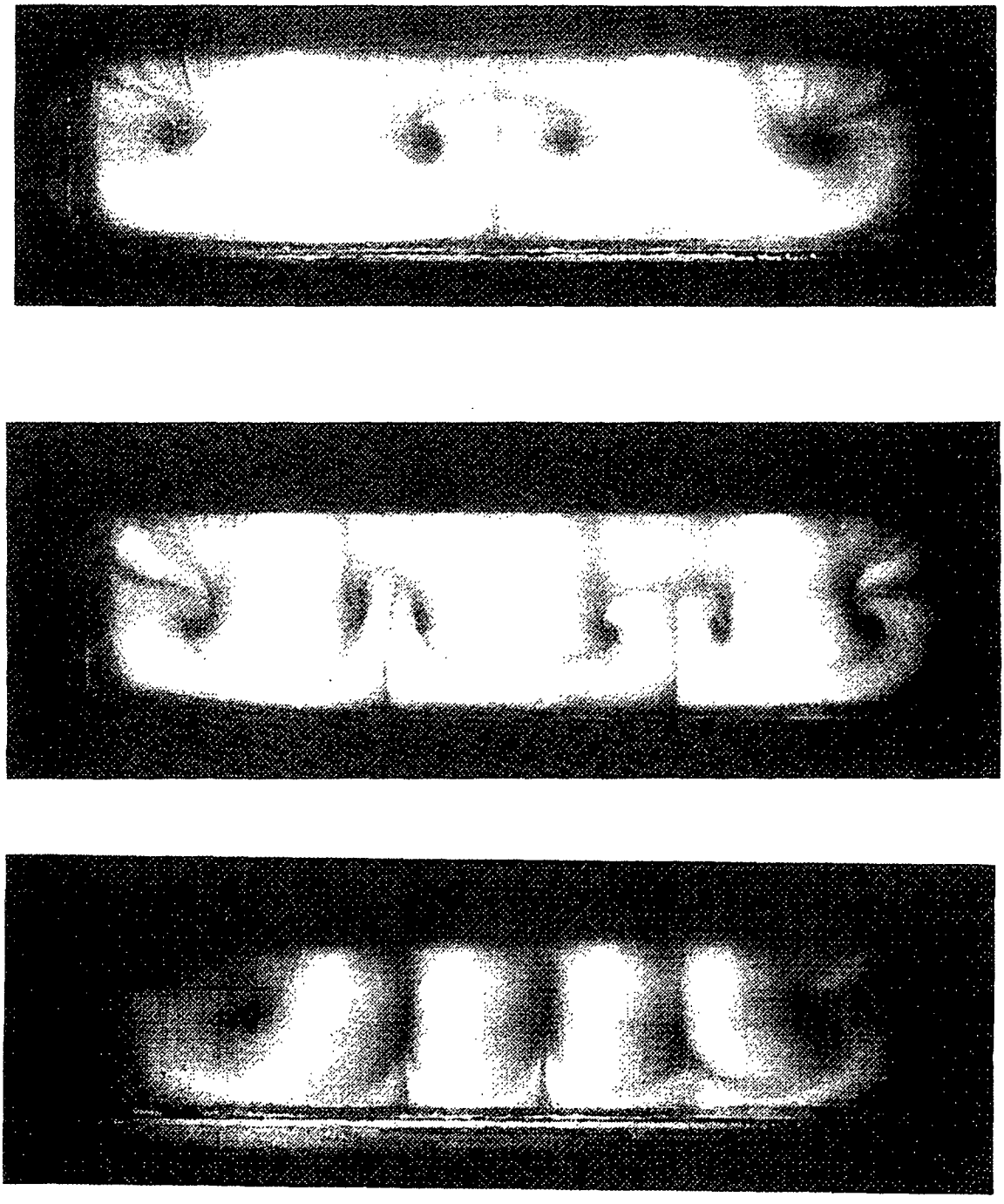

**Figure 9.** Front-view of three-dimensional flow patterns appearing at low to moderate Reynolds number (Re<300), $Re^*$=0.01-0.80.

Three-dimensional cellular structures may have two effects. First, they unevenly distribute the fluid mass and momentum transfer into the converging nip under the blade as there are alternative regions of slow and fast moving fluid elements between the cells along the spanwise direction. Second, centrifugal forces associated with recirculating patterns can induce localized variations of the solid particles concentration, thus introducing viscosity and density stratifications. Appearance of the same structures with both Newtonian and shear-thinning (e.g., coating colors) fluids is not a sufficient indication that the flow characteristics can be explained by only one control parameter--the cavity Reynolds number. Instead, the flow is really a multi-parameter system with more complex dynamics. A qualitative comparison could be useful to the extent that the viscosity value can be selected to represent the time- and shear-dependent rheology of coating colors.

The global instability of the system suggests a possible reason for the unpredictable runnability of short-dwell coaters in practice. Depending which flow pattern in the pond stabilizes first, identical operational conditions may or may not give trouble free production.

## COMPUTER MODELLING OF THE SDC POND

The isothermal, laminar two-dimensional flow of a homogeneous viscous fluid upstream of the blade nip and in the pond of a SDC coater is simulated using a general-purpose computational fluid dynamics code. The analysis presented here simulates a typical SDC pond as a 45° two-dimensional diagonal cavity and considers the bounded flow therein. After the domain of interest is discretized, the code solves the steady-state conservation equations for mass, momentum, and energy (i.e., the integral form of the governing Navier-Stokes equations) using a finite-difference method. Representation of coating color rheology is confined to the power-law model. Details about the model, its limitations, and results from numerical experiments are included elsewhere (4, 5). Here we will only review the results as they contribute to understanding the physics of the system.

Numerical results agree qualitatively with previous flow visualization experiments in the pond of a short-dwell coater (Fig. 10). Simulations indicate that the two-dimensional laminar flow in SDC ponds features curvilinear streamlines with at least two counter-rotating vortices. The more intense one is rotating clockwise and it is located close to the blade nip, thus creating the danger of separating the viscous boundary layer traveling with the moving surface and, therefore, destabilizing the momentum transfer into the nip. The second is a weaker counter-clockwise rotating one located near the bottom boundary in the region diagonally opposite to the first. These two vortices are separated by a streamline with the characteristic value equal to zero (i.e., stationary layer of fluid) which forms an effective concave surface. At high speeds and for feeding conditions of practical interest, the flow in SDC ponds is dominated by the recirculating vortex which is driven from movement of the web (or backing roll); i.e., the inflow from the feeding stream does not influence the flow in the pond. This trend was also observed in the numerical simulations by Affes, et al. (6).

The overall picture of flow, under the assumptions of the model, indicates that most fluid elements entering the pond exit by flowing over the baffle. Only elements a few millimeters away from the moving boundary (representing the web or backing roll) translate parallel to the direction of motion, thus forming

the viscous layer which enters the convergent region under the blade. Particles farther away from the moving boundary are subject to rotation as they are entrapped in the recirculating vortex. The closed zones of recirculating flows induce efficient mixing, but feature indefinite residence times. Thus, particles entrapped in this rotating motion cannot escape unless three-dimensional disturbances destabilize the vortices causing them to occasionally discharge their contents. Another feature is that the two-dimensional vortex upstream of the blade nip causes a (hydrostatic) pressure drop which, considering the relatively low pressure in the pond, may induce detrimental air entrainment. The minimum pressure inside the pond corresponds to the location of the center of the recirculating vortex.

Numerical results demonstrate that the requirements for occurrence of three-dimensional centrifugal instabilities exist in SDC pond flows. Although the simulations in this study are limited to two-dimensional flows, the significance of two counter-rotating vortices should not be underestimated. Their existence indicates, both from the theoretical and practical points of view, that this hydrodynamic system is susceptible to instabilities due to internal or external disturbances as the control parameter of the flow increases. It is well established that flows with curved streamlines develop centrifugal force-driven instabilities due to the competition between the centrifugal force and the radial pressure gradient. The unstable structures appear in the form of Taylor vortices in flow between concentric cylinders (23), and as Görtler vortices in boundary layer flow over a concave wall (24). Furthermore, such instabilities have been observed in lid-driven cavity flows (16-18), hence the geometry and two-dimensional features of flow are similar to the ones prevailing in SDC ponds.

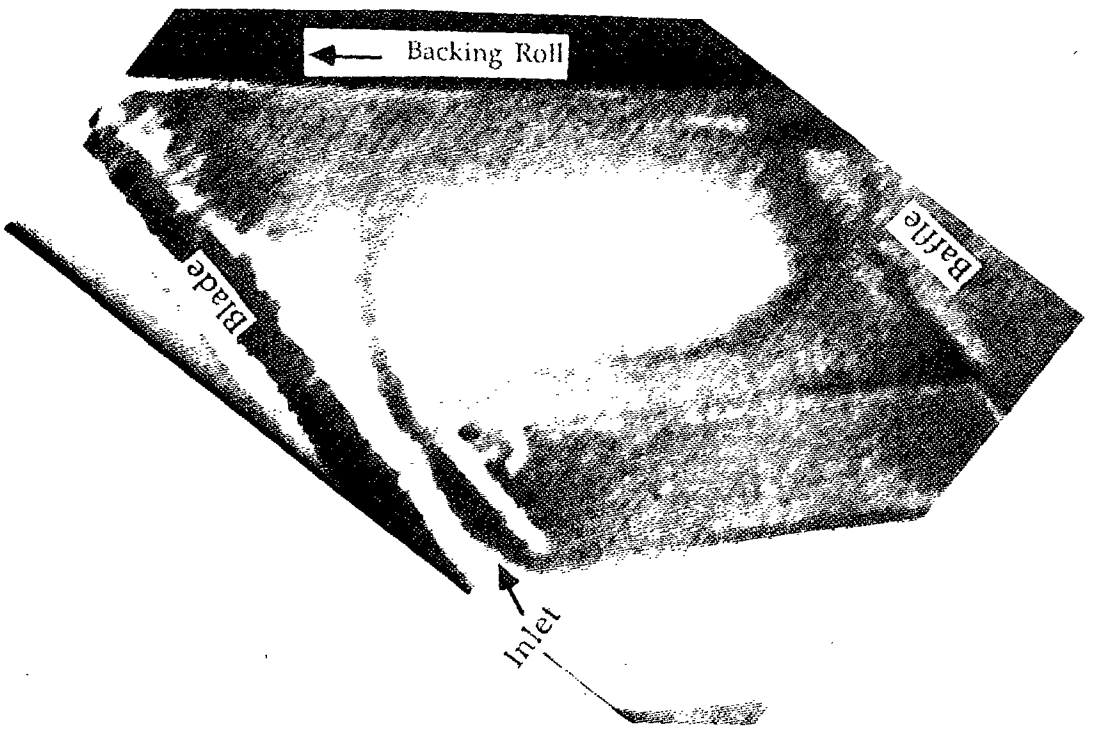


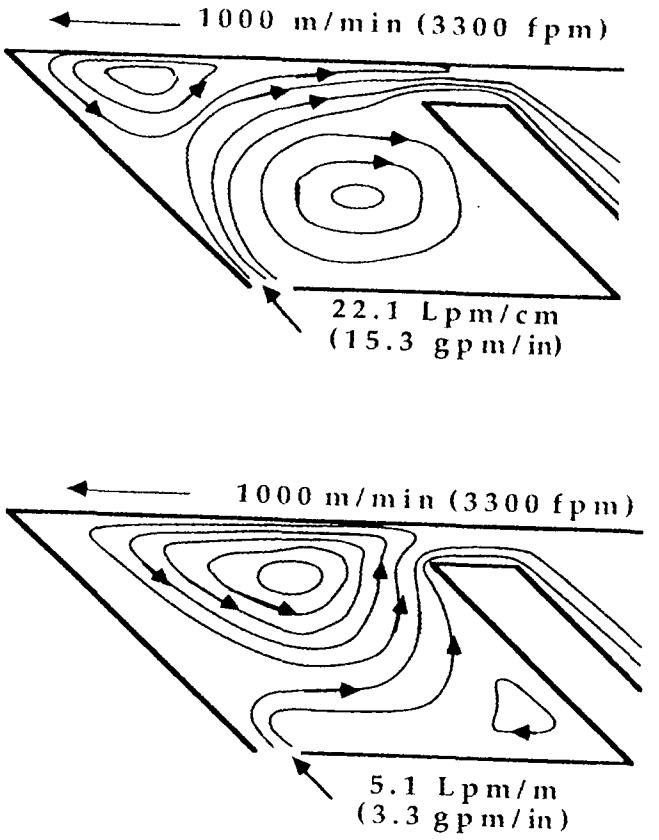


**Figure 10.** The two-dimensional flow in a short-dwell pond. The photograph is courtesy of Eklund and Norrdahl (3). The schematics represent contours of streamlines from numerical experiments at two different inflow rates.

## PILOT COATER TRIALS

### BACKGROUND

Since no systematic pilot plant data have been published with respect to the occurrence of wet streaks, the task was to collect evidence that could connect visually observed wet streaks on LWC paper with expected transitions of the pond flow. Qualitative information was obtained by inspecting the coated paper with the naked eye. The hydrostatic pressure profile (along the machine direction) normal to the roll was also measured to compile quantitative data which indirectly relate to hydrodynamic phenomena in the pond.

Pilot-plant trials were based on actual production practices, the only difference being the effective span of the coater which was only 40 cm (i.e., D/H=1, S/D=10). In all trial runs, operating conditions were adjusted to control coat weight, while the temperature of both the sheet and the color were maintained at about 27°C. Two series of trials were performed under well-controlled conditions using a 60-g/$m^2$ base stock for LWC in the first series of trials and a 50-g/$m^2$ stock in the second series. An outstanding difference between the two series was the type of delaminated clay used in otherwise similar formulations, i.e., typical for LWC papers printed with rotogravure. English China and Georgia delaminated clays were used in the first and second series, respectively. In general, because coating colors are non-Newtonian fluids, it is difficult to determine with confidence the value of the Reynolds number in complex flow fields, such as the one inside the pond. Here, to be consistent with the flow visualization experiments, we have arbitrarily chosen to base the Reynolds number on the Brookfield (100 rpm) viscosity $\mu_B$. Therefore, the parameter which defines the flow in the pond is given by an "apparent" Reynolds number $Re_a$ as:

$$Re_a = \frac{\rho V D}{\mu_B},$$

where, V is the machine speed, and D the characteristic length that defines the distance between the blade tip and the baffle. The value of $\mu_B$ was controlled by maintaining high solids levels (56-59%) to keep it from falling below approximately 900-1000 mPa.s which, from previous experience has resulted in visible streaks.

Let's look at certain rheological properties of the coating colors under consideration before we present results from trials. In particular, our efforts concentrated on formulations containing pigments with relatively high aspect ratio particles, i.e. above 15:1, such as English delaminated grades which are comprised of particles plattier than those in domestic delaminated grades of clay with aspect ratio in the range of 1:6 to 1:10 (28). In addition to 100 percent delaminated clay, the rotogravure formulation contained 3.0-4.5 pph styrenebutadiene latex and 0.3 pph alkali-swellable thickener; its total solids content was approximately 58% by weight based on dry pigment. Practical experience in both a production facility and pilot-plant trials has shown that colors with the English pigments are susceptible to wet streaking, which becomes visible to the naked eye at machine speeds above 1000 m/min.

Figure 11 demonstrates the relationship between apparent viscosity and shear rate for eleven decades of shear using four different viscometers. The data of the formulation described above are compared to a reference color, i.e., containing a domestic grade of delaminated clay at 61% solids, that had no runnability problems for machine speeds up to 1200 m/min (4000 fpm). A pressured-gas driven capillary viscometer (stainless steel capillaries, 100 mm in length, 1.03 mm in diameter) was used to collect data at shear rates of several hundred thousand reciprocal seconds, (the raw data corrected for all pertinent effects influencing the measurement). Hercules® measurements were taken with the instrument on its 'SET RPM' mode, thus minimizing temperature buildup during a test. The scattering of this data is due to the fact that all three annular gaps (with bobs A, E, and F) have been used. Brookfield data represent measurements at four different rotational speeds of the no. 3 spindle and calculation of the corresponding shear rates based on the procedure by Hyman (29). The Carimed® instrument was a controlled stress rheometer (cone-and-plate geometry) with a logarithmic stress mode. Uncertainty in the measurements with all instruments was about 10%.

Both coating colors are shear thinning over the range of shear rates from $10^{-5}$ to $10^{6}$ $s^{-1}$. Stress rheometer data illustrate that the shear-viscosity decreases by several orders of magnitude over the shear rate range of $10^{-4}$ and 10 $s^{-1}$. Comparatively, the reference color shows a similar behavior but with viscosity values at least two orders of magnitude lower. This trend was also observed when measuring the plastic yield stress from rheograms. Formulations of the color with the domestic pigment illustrated no

measurable yield value in a typical rheogram. In contrast, formulations with the problematic color had substantial yield stress in the range from 5.0 to 6.4 $x10^5$ dynes/$cm^2$ ($\pm$0.4 $x10^5$ dynes/$cm^2$). Interestingly, however, the yield stress value dropped to $1x10^5$ dynes/$cm^2$ after the color was subjected to high shear in the capillary viscometer. This suggests that structures in suspension, which are responsible for the comparatively high low-shear viscosity and yield stress of the problematic color, are sensitive to shear. Rheograms also indicated the time-dependence of viscosity in the form of a thixotropic loop.

The difference in the value of the apparent viscosity between the two colors decreases substantially with increasing shear rates, as depicted from Brookfield, Hercules, and capillary data in the shear rate range of 10 to $10^6$ $s^{-1}$. Data sets from all four instruments do not fall into a single line because of differences in the measuring geometry between the viscometers. Linear regression of the combined Brookfield and Hercules data provides the following relationship for the power-law fluid model:

$$\mu = 1.04\ \gamma^{0.56}$$

Hence, the constant 1.04 represents the so-termed zero-shear-rate viscosity limit $\mu_0$ of the color, and 0.56 is the flow index N (the regression coefficient is 0.90). The value of $\mu_0$, equal to 1040 mPa.s, is numerically similar to $\mu_B$, so that the apparent Reynolds number is roughly based on the zero-shear-rate viscosity of the color calculated with the procedure mentioned above. Thus, $Re_a$ can be conveniently calculated from measurements with two viscometers commonly used in practice. Constants $\mu_0$ and N for the reference color are 0.91 and 0.35, respectively. An outstanding difference between the reference and the problematic colors is in the flow index of the power-law fluid model. In addition to the high viscosity values observed with the stress rheometer, the problematic color has comparatively high flow index. However, the value of its flow index does not indicate shear-thickening, which is signified for N greater than one.

In review, rheological characteristics of a problematic color are: comparatively high shear-viscosity at shear rates below 10 $s^{-1}$, high yields stress, steep reduction of viscosity with increasing shear rate, and apparent viscosity comparable to the reference color in the range of $10^3$ to $10^6$ $s^{-1}$. Overall the coating color is shear-rate thinning and thixotropic with a structural viscosity which can be substantially reduced by preshearing the coating color. It should be pointed out, however, that the viscometric flows are steady

and laminar. In the practical situation of their application, coating colors are subjected to more complex hydrodynamics and other phenomena which may influence the coating process.

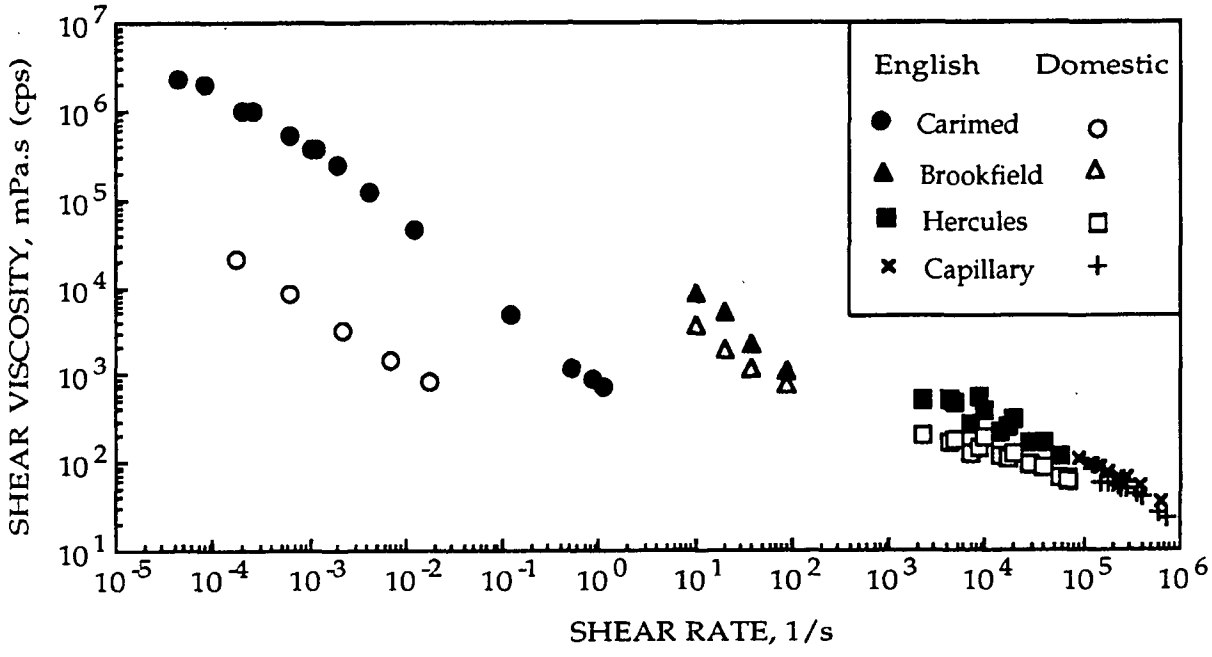


Figure 11. Rheological data of a problematic color used in pilot-plant trials and of the reference color. The first contains English China delaminated clay, the second a Georgia kaolin delaminated grade. Thermostatic temperature of Carimed and Brookfield data was 25°C; temperature of Hercules data was 20°C, and of the capillary data 22°C.

## RESULTS FROM TRIALS

Table II presents an overview of the results from the pilot-plant trials. These results should be analyzed and interpreted with caution. At first, it appears that the apparent Reynolds number of the pond, $Re_a$, is the only control parameter for the appearance of streaks. This may not be the case, as it is explained in the next section. The following paragraphs in this section report only results of the pilot-plant trials.

In both series of trials, the first occurrence of streaks appears for $Re_a$ in the range between 550 and 750. After processing, the marginal case here shows at least one streak upon visual inspection of the web (Fig. 12). Such streaks are discontinuous narrow patches of 1-3 cm in width which run along the machine direc-

tion in an intermittent and periodic manner. This is referred to in Table II as marginal appearance of wet streaks.

As machine speed increases and the control parameter $Re_a$ is raised, streaks grow both in width and frequency to eventually form almost continuous bands running along the machine direction for $Re_a$ between 800 and 1000 (Fig. 9). In their severe form, low coat weight bands cover the full CD span of the web and become visible right after the blade during high speed operations. The width of individual bands varies between 3 and 8 cm, the widest of which appears with the formulation containing the plattier clay particles, i.e., English China clay. About five to six bands are counted on a 40-cm wide web coated on the pilot SDC. At even higher speeds, the bands start a spatially oscillatory motion along the CD and, eventually, air inclusion induces skips. These nonuniformities cannot be corrected by adjusting the blade pressure (i.e., with the profile screws) across the machine line direction. Also, the problem could not be corrected by adjusting the baffle gap, the opening between the top edge of the overflow baffle and the surface of the backing roll. Interestingly, wet streaks were eliminated when the solids content of the color was reduced from 58-56 % to 52%, corresponding to a Reynolds number change from Re=760-1000 to Re=1450-2380 (baffle set at 3 mm, machine speed constant at 1000 m/min).

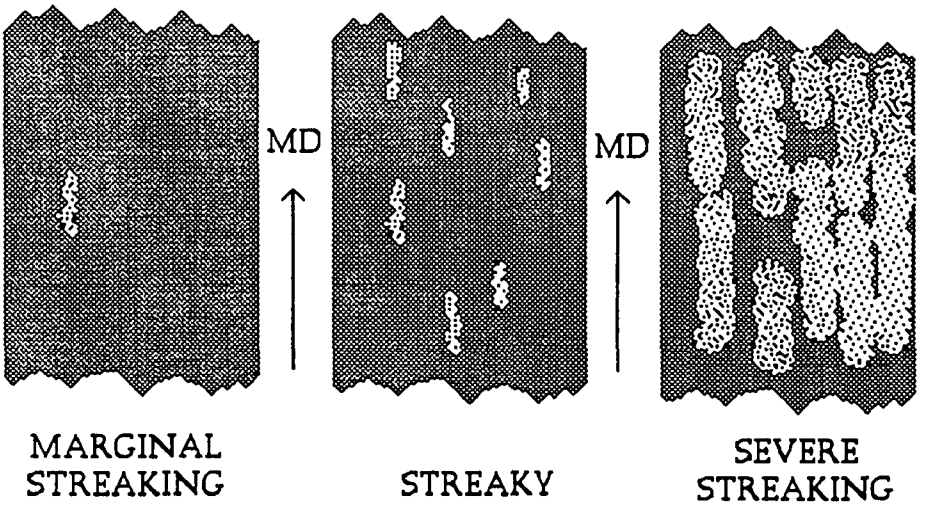


**Figure 12.** Schematic illustration of the appearance of wet streaks on LWC paper during pilot-plant trials.

**Table II.** Visual observations from LWC papers coated in a pilot short-dwell coater (45° x 0.5 x 76 mm bevelled blade, 19 mm stick-out, 3 mm baffle gap, pond D/H = 1:1, S/H = 10:1).[a]

| Trial Run No. | Color Viscosity[b] (mPa.s) | Machine Speed (m/min) | Reynolds Number $Re_a$ | Appearance of Wet Streaks |
|---|---|---|---|---|
| | | First Series ( 11 gsm, pump rate 166 L/min/m) | | |
| 1 | 1884 | 305 | 210 | No |
| 2 | 1428 | 760 | 690 | Yes |
| 3 | 1428 | 800 | 710 | Yes |
| 4 | 1428 | 820 | 740 | Yes |
| 5 | 1428 | 730 | 660 | Yes; marginal |
| 6 | 1412 | 610 | 560 | No |
| 7 | 980 | 640 | 840 | Yes |
| 8 | 980 | 670 | 880 | Yes |
| 9 | 980 | 700 | 920 | Yes |
| 10 | 1236 | 610 | 635 | Yes; marginal |
| 11 | 1236 | 700 | 730 | Yes |
| 12 | 1236 | 490 | 510 | No |
| 13 | 1236 | 550 | 570 | Yes; marginal |
| 14 | 1056 | 610 | 740 | Yes |
| 15 | 1056 | 1060 | 1300 | Yes; sever |
| | | Second Series (6-7 gsm, pump rate 166 L/min/m[c]) | | |
| 1 | 1268 | 700 | 790 | Yes; sporadic |
| 2[c] | 1292 | 305 | 670 | Yes; marginal |
| 3 | 1268 | 760 | 850 | Yes |
| 4 | 1280 | 790 | 910 | Yes |
| 5 | 1292 | 820 | 1000 | Yes |
| 6 | 1224 | 730 | 1240 | Yes |
| 7[c] | 904 | 305 | 480 | No |
| 8 | 1012 | 640 | 860 | Yes |
| 9 | 1052 | 1220 | 1650 | Yes; severe |
| 10[c] | 1004 | 1340 | 1900 | Yes; severe |
| 11[c] | 1104 | 370 | 470 | No |
| 12[c] | 1120 | 430 | 540 | No |
| 13[c] | 1156 | 490 | 600 | Yes; marginal |
| 14[c] | 1160 | 550 | 670 | Yes; sporadic |
| 15[c] | 1156 | 610 | 750 | Yes |

[a] The colors used had Brookfield viscosity of at least 900 mPa.s. Streaks do not appear at these Re values with formulations having lower viscosity.

[b] Brookfield viscosity, 100 rpm, no. 3 spindle.

[c] In this case the pumping flow rate was 200 L/min/m.

The above results suggest a connection between the appearance of streaks on the coated web and the Reynolds number, $Re_a$, for the range over which fluid viscosity and machine speed are varied. Generally, the Reynolds number decreases with reduced machine speed, but increases with lower fluid viscosity (from Eq. 1). Good examples of this are trials 6, 10, and 14 in the first series where constant machine speed at 610 m/min (2000 fpm) may or may not produce streaks depending on viscosity and the value of $Re_a$. This is also true irrespective of the type of clay pigment used, i.e., trial 15 in the second series. In the same manner, increasing machine speed while maintaining constant viscosity induces streaking, e.g., trials 4 and 6 in the first series. Thus, independent of how a certain value of $Re_a$ is attained, streaks will appear if this value is above a critical range, such as in trials 2 and 14 in the second series where $Re_a$=670 represents the marginal case for appearance of streaks.

The range of $Re_a$ over which streaks definitely occur for the first time, i.e., 550-750, is comparable with the values of Re for onset of three-dimensional flows in the experimental facility (Table I). This is true within limits imposed by experimental uncertainty and differences in geometric dimensions, especially the spanwise aspect ratio. In general, end-walls (edges) and their proximity have a destabilizing effect on the state of flow by inducing steady state three-dimensional flows(18,30). Flow in the pilot coater pond, therefore, is expected to be stable for greater values of the control parameter than in the experimental cavities. This, combined with the shear-thinning rheology of the coating color which underestimates $Re_a$, can explain differences between the critical ranges of the two parameters, Re and $Re_a$.

As the Reynolds number $Re_a$ rises above 1000-1100, streaks fill the whole CD width and are visible to the naked eye even at production speeds. This range of $Re_a$ is comparable to the critical value of Re (Table I) for which violent spanwise oscillation of the flow is observed in the experimental cavity. These conditions probably signify onset of chaotic flow in the pond, very much like the appearance of mushroom-like structures in a lid-driven cavity with through-flow.

Hydrostatic pressure measurements with a transducer mounted on the middle of the backing roll indirectly indicate existence of recirculating flows in SDC ponds. Figure 13 presents a typical profile with pressure values obtained for a wide range of color viscosities and operating conditions. Blade pressures are

estimated from the literature (14) because their range exceeds the useful range of the transducer. Measurements under conditions of practical interest show that pressure rises to 1-9 kPa (0.2-1.3 psig) right at the baffle, the greater values corresponding to narrower baffle gaps. Inside the pond and closer to the blade, a pressure drop occurs which may cause the pressure to become subatmospheric, e.g., -2 to 4 kPa (-0.3 to 0.6 psig). This drop can be explained by the existence of recirculating flows in the pond with the lowest point of pressure corresponding to the center of a vortex, something which was also confirmed qualitatively by numerical simulation. Considering the dynamics of the flow at the blade, based on the analysis by Guzy and Higgins (31) and Higgins (32), a positive drop across the blade nip puts an upper limit on the final film thickness or coat weight that can be attained. Furthermore, they show that, according to lubrication theory, below a certain film thickness the steady-state flow under the blade ceases to exist when the pressure gradient across the blade is positive. To obtain a quantitative correlation, however, between the pressure profile inside the pond and the onset of streaks, it is necessary to measure spanwise pressure variations of the viscous layer which forms at the moving surface.

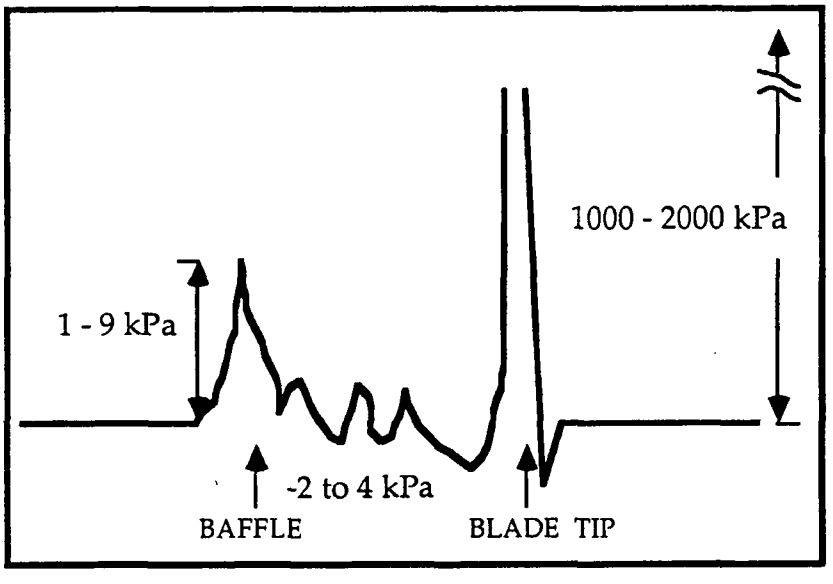


**Figure 13.** Hydrostatic pressure profile normally acting onto the backing roll inside the pond of a short-dwell coater.

## DISCUSSION AND IMPLICATION OF RESULTS

Operational differences between a bevelled blade coating system with an applicator roll and the short-dwell coater cannot only be explained by the low pressure and short contact time (between the color and the web) of the latter. The fluid dynamics upstream of the blade nip are qualitatively different between the two systems. In the case of a short-dwell coater, hydrodynamic phenomena in the pond can influence the local variation of color mass transport into the blade nip and the uniformity of the momentum transfer across the machine direction. Such phenomena may not only determine the spatial and temporal uniformity of coat weight, but can also affect orientation of inherently asymmetric pigment particles, thus explaining differences in the properties of the final coated sheet.

The laminar flow in short-dwell ponds is characterized by recirculating flows wherein strong centrifugal forces arise from curvilinear streamlines. The basic state of flow consists of a two-dimensional primary roll driven by the web, its tail-end sometimes described as a "rolling sausage" over the baffle stretching along the CD of the machine. Additional weaker (secondary) rolls appear at the corners of the pond depending on the specific geometry. This state of flow comprises the ideal case from the runnability standpoint, since there is a uniformly stable mass of fluid delivered into the blade nip across the machine direction. However, this is not a uniquely defined state because it competes with other steady states, three of which have been identified experimentally in this study. Multiple states of flow at the same Re indicate the sensitivity of the system hydrodynamic forces. Alternative states of flow feature three-dimensional structures which are stable to infinitesimal disturbances and, once established, do not switch to the basic steady state. Such behavior provides a possible explanation for the difficulty in predicting runnability in coating operations, and for the phenomenological differences between identical coaters. By analytically determining regions of attraction for each type of flow, it will be possible to set guidelines for desired operating states - useful information for production purposes.

As the fluid velocity increases, centrifugal forces cause the flow to roll up into three-dimensional evolving structures termed Taylor-Görtler-like vortices. These instabilities arise from the imbalance between centrifugal forces and pressure gradients, either inside a recirculating roll or on the layer formed

at the interface between faster- and slower-moving flows, such as those between vortices. Thus, the source of such inherent fluid dynamic instabilities is internal to the system behavior. With axes parallel to the direction of web movement, counter-rotating vortices form regions of ingoing and outgoing fluid across the blade nip which, under certain circumstances, may cause uneven CD profile. Following a series of transitional modes, the pond flow eventually reaches complex unsteady states. Incidentally, the appearance of cellular structures in the pond does not signify the onset of turbulence.

Under the conditions investigated, low coat weight streaks observed along the machine line direction relate to onset of flow instabilities in the pond of a short-dwell coater. In particular, appearance of severe streaking occurs when violent flow fluctuations set in along the span (cross machine direction) of the pond. Variations in UV reflectance (which is directly proportional to variations of coat weight as an ultraviolet dye is mixed in with the coating) of less than 2% are enough to result in a streaked see-through appearance on LWC papers coated with 6-11 $g/m^2$ on one side (33). This shows the high sensitivity of the human eye and is indicative of the difficultly in qualifying differences estimated visually.

It should be pointed out, however, that the reported results correspond to viscous coating formulations with Brookfield viscosity of approximately above 900 mPa.s (@100 rpm). Rheological measurements on the problematic color illustrate that, like most coating colors, it is shear thinning thixotropic. A primary difference from colors without any runnability problems at high machine speeds is its unusually high viscosity at shear rates below 10 $s^{-1}$ and high yield stress. Consequently, its flow behavior does not only depend on the shear rate but also the nature of the flow field. In a fully-developed rectilinear flow driven by pressure, for example, a sheared mobile layer develops next to the walls and the rest of the fluid may move as an unsheared plug. In contrast, inside confined geometries, such as the one in a lubrication flow, movement occurs simultaneously everywhere as soon as the minimum required shear stress is reached over the entire flow field. The confined flow in a SDC pond is complicated, and is often made more so by viscosity and density stratification due to recirculating flows with curvilinear streamlines and the associated centrifugal forces.

The present evidence suggests that onset of hydrodynamic instabilities in the pond may be a necessary but not always sufficient condition for occurrence of uneven CD profiles. In other words, whenever streaks are observed, the control parameter of the flow indicates unstable flows in the pond. However, it is possible for this parameter to be above its critical value without the appearance of streaks. Practical experience has shown that if viscosity is low enough (e.g., reduced solids content or smaller pigment particles), the runnability window of short-dwell coating expands with greater machine speeds.

To explain these effects, a mechanism is proposed based on results from this study. Because of the recirculating flows in the pond, fluid elements and other components of coating colors that are only a few milllimeters away from the web move opposite to the machine direction. Only after these particles have penetrated the viscous layer that forms on the moving web when the color contacts it upstream, do they experience the viscous drag of the substrate, at which point they are accelerated and convected downstream. In systems with an applicator roll, the outer layer which deflects down the blade is irrotational (1). In contrast, the flow in short-dwell coaters contains recirculating eddies, which as demonstrated above become unstable due to centrifugal forces and give rise to time-periodic and three-dimensional flow patterns. Cellular structures in the pond cause differential orientation of pigment particles and, if there is not enough time for the particles to reorient, the structures can create unstable conditions in the nip. In addition, as pointed out by Gane and Coggon (34) orientation phenomena of clay particles upstream of the blade can also affect the final coating properties. Such effects are generally more pronounced in formulations containing highly asymmetric particles, e.g., delaminated clays, at relatively high solids content. They may not , however, be important when using pigments with small particle size, e.g., a no. 2 grade of clay. Thus, CD profile variations can be attributed to the hydrodynamics in the pond coupled with color properties that are proportional to shear-viscosity. This explains why below a certain solids concentration the streaks disappear, and it also explains the appearance of streaks with larger aspect ratio particles.

## ANALYSIS OF THE CONFINED FLOW IN A CAVITY

The flow visualization experiments have revealed that different stable flow patterns can exist in the pond at the same machine speed. In other words, the flow patterns in the pond are not unique, but depending on the rate the machine is brought up to speed, flow patterns with totally different topological characteristics could form. This phenomenon is due to global instability and should not be confused with rheological hysteresis and the memory effects of viscoelastic fluids. As indicated in the previous sections, we first discovered these multi-stable three-dimensional patterns using Newtonian fluids.

Since the existence of multi-stable operating states revealed by our flow visualization experiments have broad and significant implications in coating systems, it is important to establish a firm theoretical basis to understand and interpret the results. In this section, we prove the existence of the multi-stable states based on fundamental fluid dynamics principles followed by a theoretical explanation of the results using nonlinear dynamical analysis and topological arguments based on critical point theory. Specifically, we prove that (a) the flow patterns observed in the flow visualization experiments shown in Fig. 9 are topologically different and therefore represent distinct steady states, and (b) these steady state flow patterns are unstable to finite-amplitude disturbances.

Due to the complex nature of the three-dimensional flow patterns that are observed in the experiments, it is difficult to conceptually visualize their structures. Very often, two patterns which appear different due to lighting effects or different visualization techniques used in the experiment, may in fact represent identical flow states. A topological description of the flow patterns based on critical point theory provides a framework and methodology for avoiding this difficulty. A three-dimensional flow pattern can have one or more critical points which are defined as points in the flow field where the fluid velocity goes to zero (stagnation or separation points) and the slope of the streamlines become indeterminate. Several types of critical points are identified depending on how the streamlines form. Stable and unstable *foci* and *nodes*, and *saddle* points shown in Fig. 14 are the most common critical points. There are also degenerate or borderline cases such as *pure shear and center points*.

A flow field can be uniquely characterized once all of its critical points are correctly identified. In an experimental approach, as in this study, these points are identified by tracing the streamlines with various visualization techniques. In a computational approach, however, a Taylor expansion of the velocity, in terms of the space coordinates and subsequent analysis of the leading terms, provides complete information about the points.

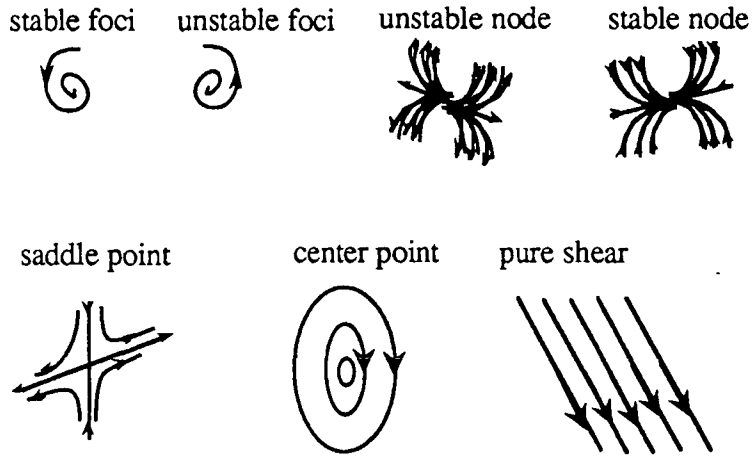


**Figure 14.** Classification of critical points of the flow field inside the pond of a short-dwell blade coater.

For illustrative purposes, let us first analyze the two-dimensional lid-driven cavity flow field on the AEFG plane represented by Fig. 4. Because of its limited degree of freedom, a two-dimensional flow pattern can only consist of centers and saddles. Each of the primary and secondary vortices form a center which essentially consists of a stagnation point at the center of closed streamlines. The interface between the primary and secondary vortices is a separation line which connects two saddle points on the no-slip boundary (wall) of the cavity, as shown in Fig. 15. Therefore the two-dimensional cavity flow of Fig. 4 contains four center points (the primary eddy plus three secondary vortices) and six saddle points (two for each secondary vortex).

The analysis of a three-dimensional pattern is considerably more involved. It is usually more productive to consider the projection of a three-dimensional pattern onto a two-dimensional plane. Let us first

examine the three-dimensional pattern at the top of Fig. 9. Here, the flow is symmetric with respect to the centerline of the cavity. The symmetry line consists of two saddle points; one at the no-slip bottom wall (at the center of the bottom plane), and the other one about the center of the cavity, as shown in Fig. 16a. Note the difference between a complete saddle point inside the flow and one formed on a no-slip boundary. There are two stable foci on each side of the symmetry line, and each side-wall contains a no-slip boundary saddle. Also, the bottom wall contains two additional boundary saddle points on each side of the symmetry line. Thus, the first three-dimensional flow pattern consists of one saddle, five no-slip boundary saddle points, and four stable foci. We call this flow pattern a *2-cell* structure.

The second pattern at the middle of Fig. 9 is a *3-cell* structure where each cell contains two stable foci and a no-slip boundary saddle at the bottom border. There is a saddle and a no-slip boundary saddle between each cell, and a no-slip boundary saddle on each side-wall. Therefore the 3-cell structure contains six stable foci, two saddles, and seven no-slip boundary saddles as illustrated in Fig. 16b. Similarly, the *4-cell* structure at the bottom of Fig. 9 contains eight stable foci, three saddle points, and nine no-slip boundary saddle points (Fig. 16c). The foci in the 4-cell structure are not as clearly distinguishable as the ones in the other two flow structures.

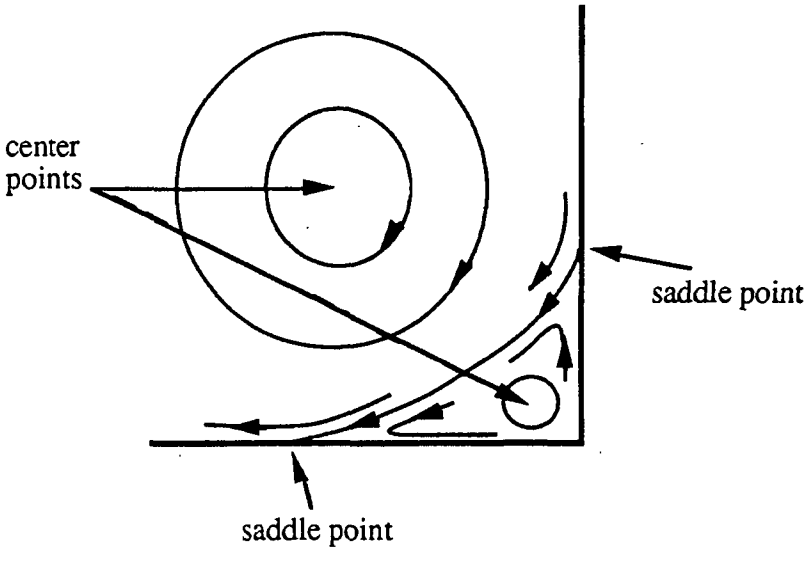


**Figure 15.** Critical points in a two-dimensional cavity flow.

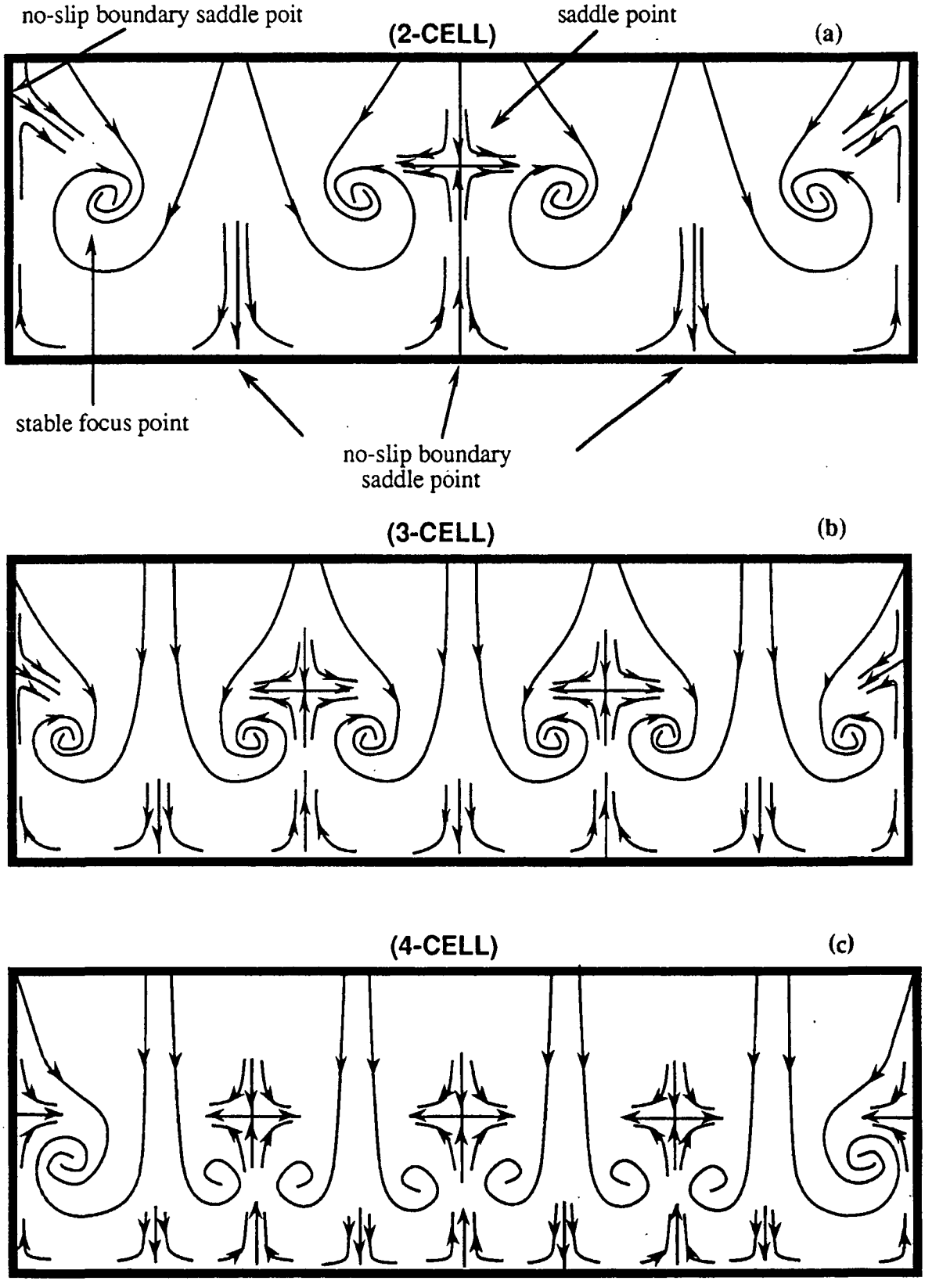


**Figure 16.** Topological characterization of the three-dimensional patterns basedon critical-point theory. The 2-cell (a), 3-cell (b), and 4-cell (c) structures correspond to the three patterns presented at the top, middle, and bottom of Fig. 9, respectively.

From this analysis we conclude that the patterns in Fig. 9 each have distinct topological characteristics and therefore are different steady states that could stabilize in the pond of a short-dwell coater. We also expect that their influence on the runnability and the momentum transfer under the blade would be different. However, before we can state with absolute confidence that different flow patterns can form in the pond under identical operating conditions, we should resolve the following question: Do the fundamental principles of physics governing the motion of a fluid permit multi-stable flow patterns in such a system? The following paragraphs address this question.

Let us begin with the simplest case -- a lid-driven cavity (LDC) with width aspect ratio D/H = 1 (cavity depth, H, is used as the length scale) and infinite span. The Navier-Stokes and Continuity equations given by:

$$\underset{\sim}{u}_{,t} + Re\,(\underset{\sim}{u} \cdot \nabla \underset{\sim}{u}) = \nabla p + \nabla^2 \underset{\sim}{u} \qquad \text{in} \quad \Omega \qquad (1a)$$

$$\nabla \cdot \underset{\sim}{u} = 0 \qquad \text{in} \quad \Omega \qquad (1b)$$

govern the flow in the cavity domain defined by $\Omega$. The velocity vector, $\underset{\sim}{u}$, pressure, p, and time, t, are scaled with the lid velocity, V, pressure scale, $\mu V/D$, and time scale, $D^2\rho/\mu$, respectively. The Reynolds number, Re, defined as $VD\rho/\mu$ is the only parameter in this problem. The boundary conditions are no-slip walls, given by:

$$\underset{\sim}{u}\,|_{\partial\Omega_t} = (V,0,0) \qquad \text{and} \qquad \underset{\sim}{u}\,|_{\partial\Omega - \partial\Omega_t} = (0,0,0) \qquad (2)$$

where $\partial\Omega$ is the boundary of $\Omega$ and $\partial\Omega_t$ represents the top surface. At a sufficiently small value of Re, the solution to this system represents a two-dimensional (2-D) flow given by:

$$\underset{\sim}{u}_{2D} = [\, u(x,y),\, v(x,y),\, 0\,] \qquad (3)$$

This solution is available for creep flows in closed form by Pan and Acrivos (35), and in numerical form for a wide range of Re by many investigators (for example, see Bozeman and Dalton (36); or Nallasamy and Prasad (37)). In practice, however, this solution becomes unstable at a critical Reynolds number, $R_c$, and most likely gives rise to a steady cellular flow through a pitchfork bifurcation (38). The value of $R_c$ and the wavelength of the critical mode, $l_c$, depend on the depth-to-width aspect ratio. The three-dimensional (3-D) solution near onset can be approximated by separating variables in the linearized

disturbance equation and using trigonometric representation in the z-direction. The critical disturbance at onset is then given by:

$$\underset{\sim}{u}' = [\, u'(x,y)\, \cos Z,\ v'(x,y)\, \sin Z,\ w'(x,y) \sin Z \,] \qquad (4)$$

where $Z = 2\pi(z-\alpha)/\lambda$, $\lambda$ is the wavelength of the periodic cellular flow, and $\alpha$ represents an arbitrary phase of the disturbance structure.

Now consider a cavity with finite span, L, and slippery end walls. The boundary conditions at the end-wall planes, $\partial\Omega_e$, are given by:

$$w = 0 \qquad \text{and} \qquad \frac{\partial u}{\partial z} = \frac{\partial v}{\partial z} = 0 \qquad \text{on} \qquad \partial\Omega_e \qquad (2')$$

Here also the steady two-dimensional solution (3) satisfies the boundary conditions (2'). The bifurcating 3-D solution at onset can be represented by (4) with the eigenfunction modified to $n\pi z/L$, where n is the wavenumber of the destabilizing disturbance structure inside the container, and the phase angle, $\alpha$, being no longer arbitrary, is set to zero. Modes representing an even or odd number of cellular patterns can become critical and destabilize the 2-D base solution as shown in Fig. 17. Here the vertical (horizontal) plane represents solutions with an odd (even) number of cellular patterns.

Since the slip condition at the end wall given by (2') is also a symmetry condition, the similarity mapping used by Aidun (39) applies. Therefore, by calculating the stability boundary for a single-cell pattern, $R_c^1(L)$, the entire stability boundary for the initial bifurcation point for n-cell patterns can be mapped using transformation: $R_c^n(L) = R_c^1(L/n)$ where $n=1,2,\ldots$

The expected form of the stability boundary predicted by Eq. (5) is shown in Fig. 18.

Let us next discuss the real LDC system where the no-slip condition applies to the end walls as well as to any other solid boundary. Previous studies assume that if the span-to-width aspect ratio is equal to or greater than unity, then the wall effects are insignificant and the flow is two-dimensional. Since these assumptions are fundamentally incorrect and can lead to erroneous conclusions in practical problems, even at a small Reynolds number, it is appropriate to examine this in some detail.

The no-slip condition generates an Eckman-type viscous layer at the end walls which results in a radially inward motion of the fluid toward the center of the primary eddy near the wall. This can be

demonstrated by application of the radial component of Euler's equation to the circular streamlines near the viscous layer. The radial pressure gradient, $\frac{\partial p}{\partial r}$, is balanced by the centrifugal acceleration $\frac{\rho U^2}{r}$, where U is the circumferential velocity of the fluid. For a fixed pressure gradient, velocity U becomes smaller as the fluid particles approach the end walls. Therefore, to keep the balance, fluid particles must follow a circular path with a smaller radius[a], r. To keep the mass balance, the fluid at the center of the primary eddy near the wall is then forced away toward the center symmetry plane where it flows radially outward and completes a loop. The three-dimensionality of the flow is vividly apparent even at Re as low as 100 where the de Val Davis and Mallinson (42) numerical solution shows this general flow pattern.

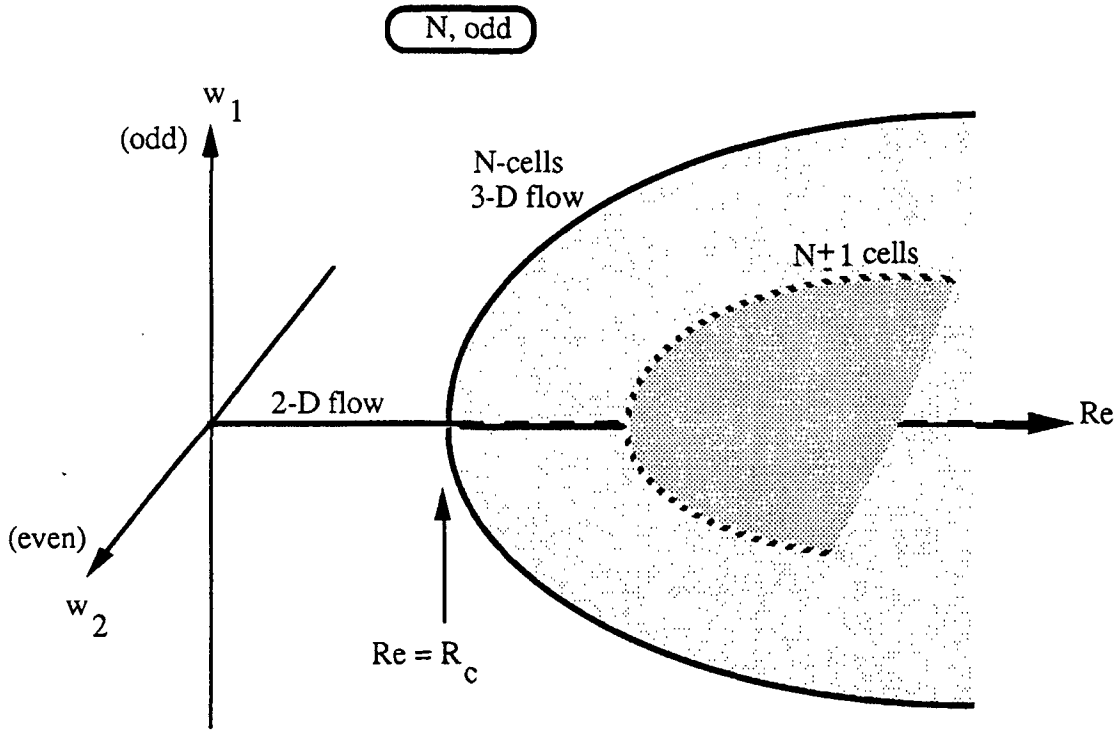


**Figure 17.** State diagram for an ideal lid-driven cavity with slippery end-walls.

---

a) Bödewadt's (40) solution (see Schlichting (41)) of a semi-infinitely long eddy contacting a stationary solid surface shows an overshoot in tangential velocity near the wall which has also been verified experimentally and would approximate the flow here.

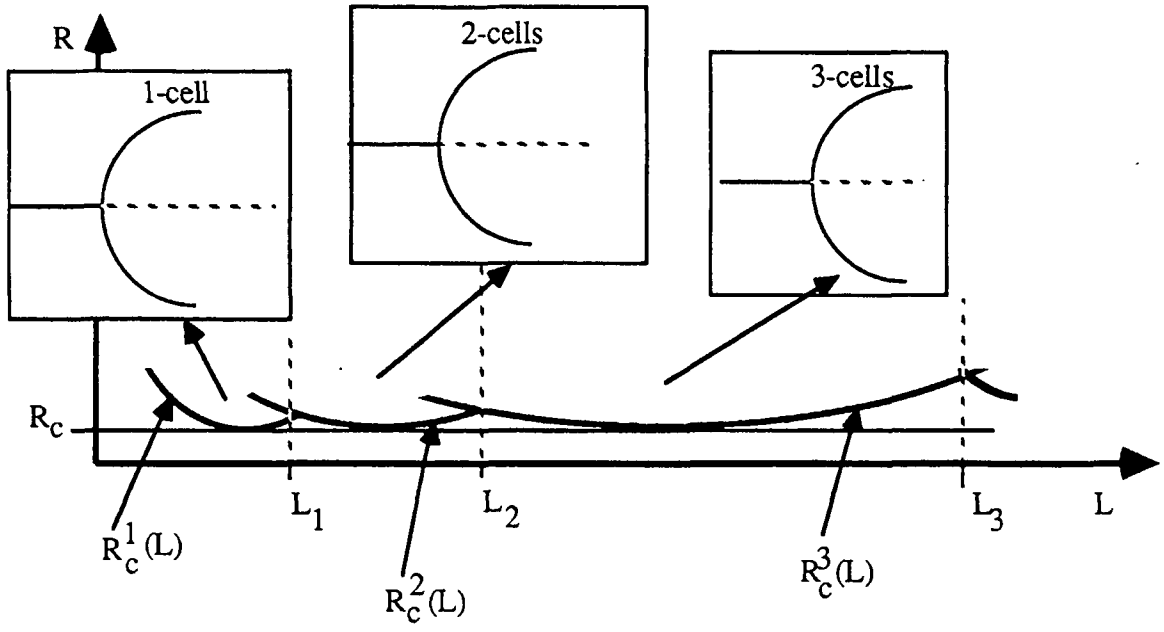


**Figure 18.** An example of the stability boundary and corresponding critical modes as a function of the span length, L.

To construct the bifurcation diagram for the 3-D cavity flow, we outline the following principles: (a) the pitchfork bifurcation diagrams of the ideal flow in Fig. 17 and 18 are not generic and therefore almost any perturbation of the system will change their qualitative appearance; (b) there exists a positive real number , $\varepsilon$, where, for $Re<\varepsilon$, the solution to the governing equations along with the no-slip boundary conditions is unique and unconditionally stable (43); and (c) the Leray-Schauder (L-S) degree theory applies, that is, except at bifurcation points, the total number of solution branches at a given value of Re is odd and the summation of the L-S indices for stable (-1) and unstable (+1) solutions will be unity (44).

Given these facts, and considering the addition of no-slip as a perturbation of the ideal system, we expect the pitchfork bifurcation to decouple in the standard manner represented in Fig. 19. The decoupling generates two stable steady states and one unstable branch through a turning point satisfying the conditions outlined above. The first steady branch which represents the only solution near Re=0 is the *primary* state, and it represents a three-dimensional flow as soon as it forms at Re=0. The other stable solution, the secondary mode, represents a second steady flow which destabilizes through a turning point at $Re=R_{TP}$. The secondary state can exist only at $Re>R_{TP}$ and is replaced by the primary state for lower values. The

other cellular branches of the ideal system of Fig. 17 also decouple and result in additional locally stable modes. The patterns in Fig. 19 represent the decoupled secondary modes resulting from perturbations of the cellular patterns of the ideal system.

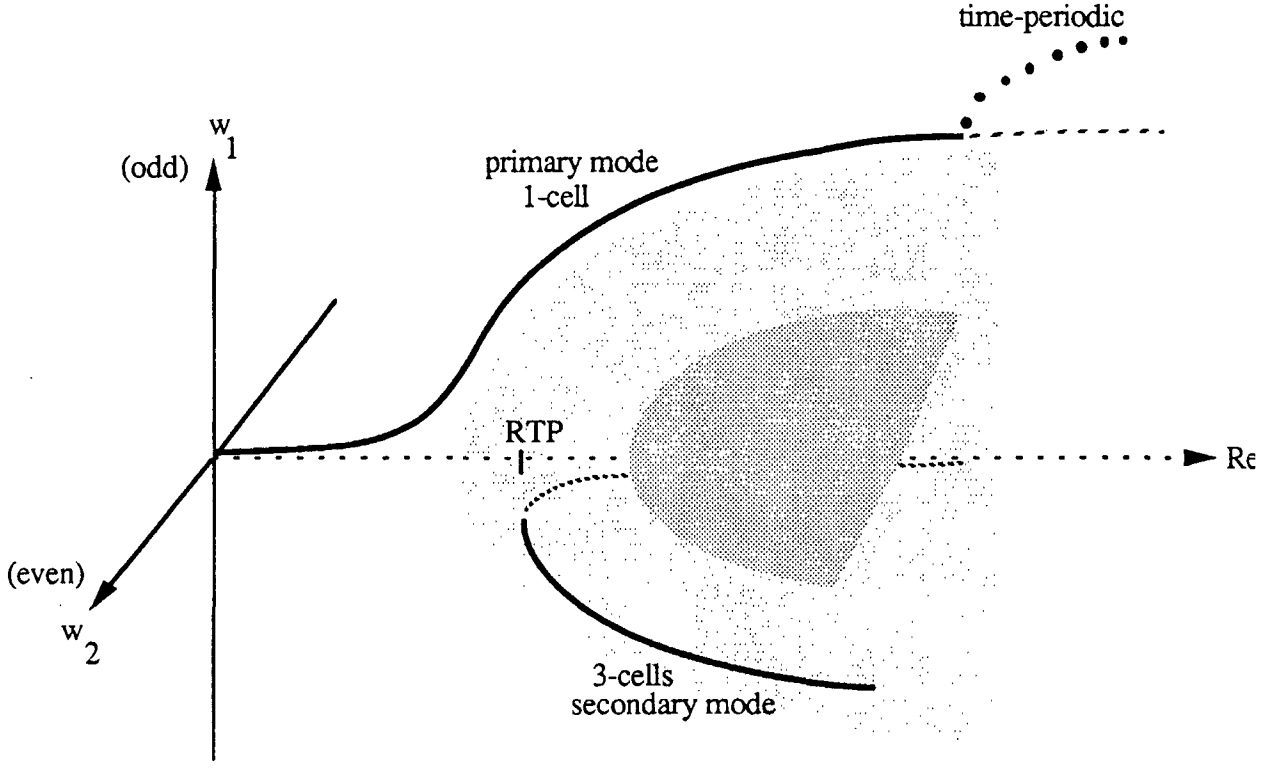


**Figure 19.** Decoupling of a pitchfork bifurcation for a three-dimensional lid-driven cavity.

The bifurcation sequence and the stability characteristics of flow in a LDC proposed above remain to be proved or modified through rigorous analysis. To study problems which are a subclass of the LDC system (e.g., coating and other surface application systems), requires a fundamental understanding of flow in a LDC. At this time, we base the discussion of our experimental results on the above theory.

As indicated above, the difference between the through-flow cavity studied here with a closed LDC is the additional parameter, $Re^*$. For a fixed geometry, the problem considered here is really a two-parameter system and therefore, unfolds the bifurcation diagram of Fig. 19. However, since results do not change qualitatively in the range of $Re^*$ considered in our experiments, we assume that the through-flow

serves as a perturbation of the LDC; that is, we assume that all of the principles outlined above also apply here. Furthermore, we note that the bifurcation diagram of Fig. 19 is generic and therefore perturbations of it do not necessarily result in qualitative changes.

Given the above facts and assumptions as a framework, we can identify the sequence of states in Fig. 5 as transitions in the primary mode. Fig. 5a represents the steady state primary mode, a three-dimensional flow, which consists of primary and secondary corner eddies. This state, which we refer to interchangeably as either the *primary state* or the 1-cell pattern, is the well-known LDC flow. Our flow visualization experiments show that this state loses stability at Re~500 and gives rise to a time-periodic flow (Fig. 5b) as shown by the state diagram in Fig. 20. It appears that the disturbance structure is in the form of a spiral vortex which superimposes on the base state and is responsible for this transition.

Although flow visualization methods used in these experiments cannot provide the detailed information required to establish the higher order transitions, some information can be extracted through observation. At Re~600, the interface between the primary and the DSV becomes wavy and the spiral-shaped vortex on the DSV appears to fold over itself and develop spikes (Fig. 5c). It is not clear whether this signals transition into a different periodic state. At higher Re, the flow develops a bursting character in the region of the DSV, a clear signal of higher order transitions. In the neighborhood of Re~1000, mushroom-shaped structures form and burst rapidly in alternating positions. These structures are almost identical to the cross-sectional view of Görtler vortices observed and recorded in boundary layer flow over concave surfaces (for example see Peerhossaini and Wesfreid (27)). These vortices in LDC systems have also been studied by Koseff and Street (17) and Prasad and Koseff (18) who have made extensive Laser-Doppler Velocimeter measurements at discrete values of Re. They focus on the transition to turbulence which they show occurring at Re>6000. These and other studies have focused only on the primary state of flow in LDCs. In fact, to our knowledge secondary stable modes have never been reported in this system.

Our experiments show that in a LDC system (with depthwise and spanwise aspect ratios of 1 and 3, respectively, and with a small amount of through flow) the primary stable steady state (Fig. 5a) is only locally stable and competes with at least three other secondary steady state modes, each having a unique and qualitatively different flow pattern as shown in Fig. 9. All of these patterns remain symmetric with

respect to the mid-plane by forming 2-, 3-, and 4-cell structures. These structures have been observed in the range of 250<Re<350. We identify these states with the decoupled n-cell branches of the ideal system (Fig. 18) which may form and mutate in various ways. An example of one of the possible arrangements is shown in Fig. 20.

To summarize the results from this section, we have (a) proved that the fundamental laws of physics allow for multi-stable steady states to exist in the pond of short-dwell coaters, and (b) with the aid of nonlinear dynamical analysis, explained the mechanism by which these competing steady state patterns can form.

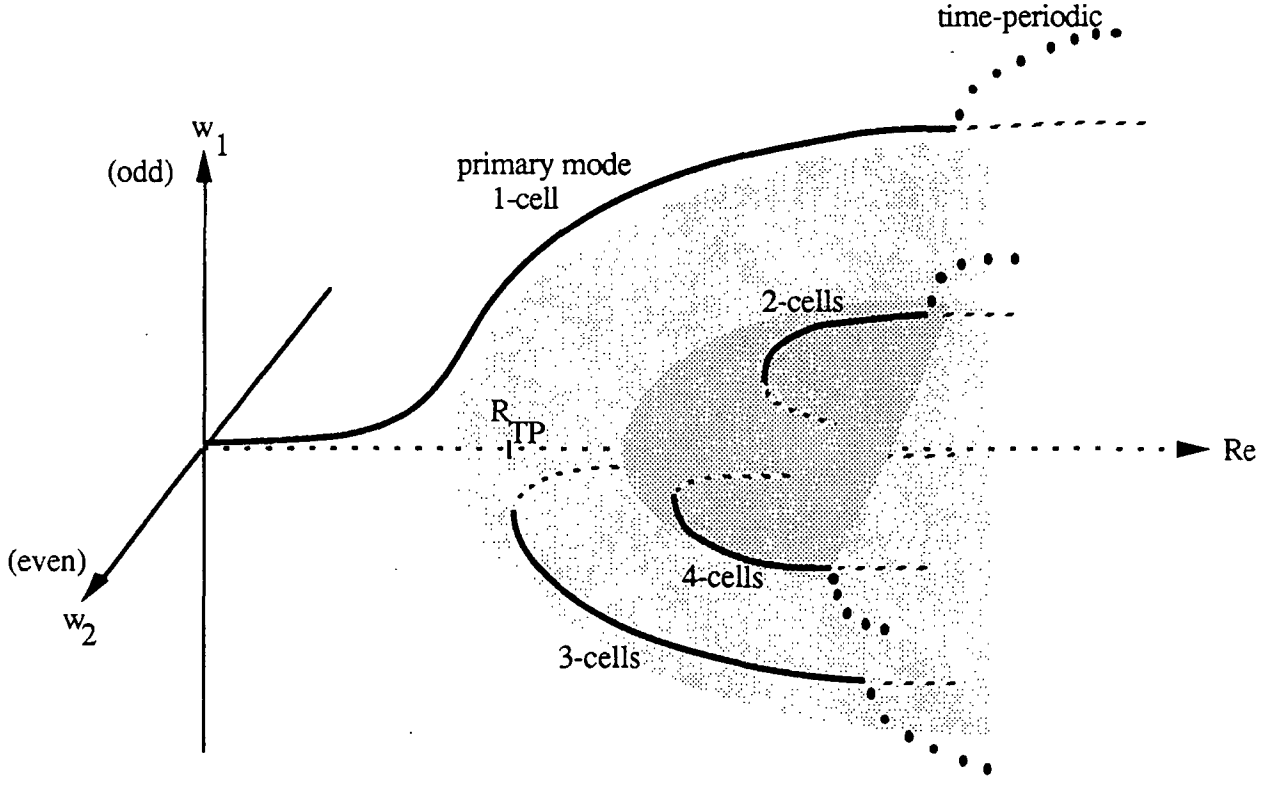


**Figure 20.** Example of a possible state diagram for a lid-driven cavity with through-flow.

## RELEVANCE OF RESULTS TO THE INDUSTRY:

## RETROSPECTIVE AND OUTLOOK

As the trend in coating technology shifts toward higher machine speeds and lower coat weights, it is recognized that film thickness imperfections put an upper limit on machine speed and/or solids content of the coating color. This is especially important when using large, highly orientable pigment particles which give better print quality but their application is not conducive to high solids content. In this study, we have shown that speed limitation originates from unstable flows in short-dwell coater ponds. Such flows result in differential momentum transfer through the blade nip and subsequent appearance of streaks.

The work presented here pinpoints the physical origin of the problem which limits the operational speed of blade coaters and affects product quality. Although this study has focused on short-dwell coaters, the results apply to the broad class of thin film processing systems which involve shear-driven recirculating eddies. Many surface systems for web modification - such as puddle and roll coaters, modern surface sizing presses and printing presses - share similar hydrodynamic characteristics and, therefore, suffer from similar nonuniform metering variations at high machine speeds.

Dynamical behavior and instability are naturally affecting many processes in papermaking and converting (45). The unique experimental and theoretical techniques developed throughout the course of this study provide the tools for investigation of flow instabilities in other papermaking processes such as centrifugal cleaners, headboxes, and the forming section in general. Unveiling the mechanisms which induce and control these phenomena would contribute to effectively predicting and controlling these processes, while consistently manufacturing products with superior quality at high machine speeds.

## CONCLUSIONS

Results from experimental, computational, and theoretical studies presented here provide a new insight regarding the fluid dynamics of this class of surface application systems. First, it has been revealed that such hydrodynamic systems have multiple, stable but competing, operating states under the same conditions. Second, the system becomes unstable as machine speed continually increases, featuring three-dimensional flow structures. At high machine speeds, the flow in the pond is controlled by the recirculating eddy induced from the movement of the web rather than the inflow. Due to the curved streamlines of this flow, the system is susceptible to centrifugal instability in the form of Taylor-Görtler vortices. Pilot-plant trials with short-dwell coaters indicated that onset of these flows is associated with appearance of wet-streaks.

Specifically, flow visualization in a lid-driven rectangular cavity with through-flow and finite dimensions, which experimentally simulates the short-dwell pond, reveals previously unknown aspects of such flows. These are:

1. The two-dimensional state, the ideal flow pattern for coating, competes with multiple steady states having three-dimensional flow structures. Three competing states have been identified to date. These are stable states in the sense that once established they do not switch into the basic two-dimensional state. The nonunique nature of steady flows can possibly be the cause of the difficulty in predicting runnability in many practical situations.

2. When the Reynolds number - the control parameter of the flow based on cavity width and fluid Brookfield viscosity (@ 100 rpm) - increases, centrifugal instabilities set in in the form of Taylor-Görtler-type vortices, pairs of counter-rotating rolls with axes parallel to the machine direction. The vortices meander along the span of the cavity, progressively oscillating, and eventually evolving into more complex states. There is little doubt that similar vortices appear in the pond of short-dwell coaters and other confined-flow geometries of size press equipment. Regions between these vortices are characterized by differential mass transport and uneven momentum transfer into the blade nip. Critical values of the control parameter for onset of the various transitional modes of flow have been identified for square cavities with a span-to-width aspect ratio of 3 to 1.

Trials in a pilot-plant SDC facility with coating colors having problematic runnability showed the following:

1. Within the range over which the fluid viscosity was varied, appearance of streaks on LWC papers correlates well with expected onset of hydrodynamic instabilities in the pond. For a pilot coater having a span-to-width ratio of 10 to 1, streaks appear in their marginal form at $550<Re_a<750$ and in their severe form at $Re_a$ greater than 1100. These results indicate that pond hydrodynamics constitute an important factor affecting runnability of high-speed SDC coaters.

2. However, these results are based on viscosity values of at least 900 mPa.s attained, for example, when processing formulations containing large proportions of delaminated clays at high solids content. These colors are shear thinning thixotropic, but demonstrate unusually high low-shear viscosity and yield stress. For colors having lower viscosities or solids content, the streaks actually disappear although the Reynolds number will be higher. Thus, onset of instabilities constitutes a sufficient but not always necessary requirement for appearance of streaks.

This study increases the understanding of this class of problems and proves, with concrete evidence, the existence of some new flow instability issues which influence the operation of short-dwell coaters and other equipment for web modification with similar hydrodynamic characteristics.

ACKNOWLEDGEMENTS

This work is primarily supported by the member companies of The Institute of Paper Science and Technology (IPST) through Project 3674 - Fundamentals of Coating Systems. The equipment for laboratory simulation of the short-dwell ponds is donated to IPST by Beloit Corp., which also contributed time and manpower for the pilot-plant trials. Portions of this work will be used by N. G. T. as partial fulfillment of the requirements for the Ph. D. degree at IPST. Portion of this work was originally published in Tappi Journal, June 1990, ©TAPPI 1990.

LITERATURE CITED


1. Pranckh, F. R., Scriven, L. E., The Physics of Blade Coating of Deformable Substrate. Coating Conference Proceedings. TAPPI Press, Atlanta, GA, 1988, pp. 217-238.

2. Eklund, D.E., Strömberg, M., Das Strömungsbild beim Short-Dwell-Blade-Strichauftrag. Wochbl. Papierfabr. 114(6):203-205(March 1986).

3. Eklund, D. E., Norrdahl, P. C., The Flow Characteristics in a Short Dwell Coater. Coating Conference Proceedings. TAPPI Press, Atlanta, GA, 1986, pp. 99-102.

4. Triantafillopoulos, N.G., Rudemiller, G., Farrington, T., Lindsay, J., Numerical Simulation of Short Dwell Pond Flows. Engineering Conference Proceedings, Book 1, TAPPI Press, Atlanta, GA, 1988, pp. 209-218.

5. Triantafillopoulos, N.G., Rudemiller, G., Aidun, C., Numerical Experiments of Short Dwell Coater Pond Flows, Int'l Symposium Pigment Coating Structure and Rheology. INSKO, Helsinki, Finland, Feb. 8-9, 1989.

6. Affes, H., Conlisk, A.T., Foster, M.R., The Steady Flow in a Short-Dwell Coater. Coating Conference Proceedings. TAPPI Press, Atlanta, GA, 1990, pp. 299-308.

7. Aidun, C., Principles of Hydrodynamic Instability in Coating Systems. Coating Conference Proceedings. TAPPI Press, Atlanta, GA, 1990, pp. 275-298.

8. Korpela, M., Palsanen, J., Pitkanen, S., Practical Experience with SDTA. Wochbl. Papierfabr. 114(8): 267-271(April 30, 1986).

9. Beisswanger, R., Coating Paper and Board, Practical Experience with the Short-dwell and Long-dwell Time Applicators. Blade Coating Seminar Notes. TAPPI Press, Atlanta, GA, 1986, pp. 137-143.

10. Baumeister, M., Experiences with Short-Dwell Coating Aggregates. Coating 19(11):384-387(Nov. 1986).

11. Ruckert, H., Sommer, H. -P., Development of a Coating Device for Low Coating Weight at High Production Speed and High Solids Content. Wochbl. Papierfabrik. 114(5) :141-147(March 15, 1986).

12. Sommer, H. -P., Applicating Systems for Coating Ultra-lightweight Coated and Machine Finish Pigmentized Papers. Coating Conference Proceedings. TAPPI Press, Atlanta, GA, 1988, pp. 131-137.

13. Baumeister, M., European Coating Technology. Pulp Paper Can. 90(3):T100-T111(1989).

14. Sollinger, H.-P., Dynamic Coater -seine Auftrags- und Egalisiersysteme. Wochbl. Papierfabrik. 117(8):332-338(April 1989).

15. Triantafillopoulos, N., Aidun, C. Relationship between Flow Instability in Short-Dwell Ponds and Cross Directional Coat Weight Nonuniformities. Tappi, 73(6):127-136(June 1990).

16. Koseff, J. R., Momentum Transfer in a Complex Recirculating Flow. Doctoral Dissertation. Department of Civil Engineering. Stanford University, CA, 1983.

17. Koseff, J.R., Street, R.L., Visualization Studies of a Shear Driven Three-dimensional Recirculating Flow. J. Fluid Eng. 106(3):21-29(March 1984).

18. Prasad, A.K., Koseff, J.R. Reynolds Number and End-wall Effects on Lid-driven Cavity Flow. J. Fluid Eng. 106(3):21(1984).

19. Triantafillopoulos, N. G., Fluid Dynamics in Short-Dwell Coater Ponds. Ph. D. Dissertation. Progress Report 10. May 1989. The Institute of Paper Science & Technology, Atlanta, GA.

20. Quraishi, M.S., Fahidy, T. Z., Techniques for Flow Pattern Studies. In Encyclopedia of Fluid Mechanics. Chapter 28. (N. P. Cheremisinoff, ed.) Gulf Publishing Co., Houston, TX, 1986, pp. 811-840.

21. Mueller, T.J., Flow Visualization by Direct Injection. In Fluid Mechanics Measurements. Chapter 7. (R. J.Goldstein, ed.) Hemisphere Publishing Corp., Washington, DC, 1985, p. 354.

22. Triantafillopoulos, N.G., Farrington, T.E., Flash X-ray Radiography Techniques for Visualizing Coating Flows. Coating Conference Proceedings. TAPPI Press, Atlanta, GA, 1988, pp. 47-51.

23. Taylor, G.I., Stability of a Viscous Liquid Contained Between Two Rotating Cylinders. Phil. Trans. Royal Soc. London, Series A 223 :289-343(1923).

24. Görtler, H., Nachr. Akad. Wiss. Göttingen, Math. Phys. Kl. 2 (1940); translated as "On the Three-dimensional Instabilities of Laminar Boundary Layers on Concave Walls". Tech. Memorandum 1375, NACA, 1954.

25. Kottke, V., On the Instability of Laminar Boundary Layers Along Concave Walls Towards Görtler Vortices. In Propagation in Systems Far from Equilibrium. Springer-Verlag, New York, NY, 1988, pp. 390-398.

26. Aidun, C., Triantafillopoulos, N.G., Global Stability of the Flow in a Short Dwell Coater Pond. Paper presented at the International Conference of Thin Films Mechanics, Orlando, FL, 1990.

27. Peerhossaini, H., Wesfreid, J.E., Experimental Study of the Taylor-Görtler Instability. In Propagation in Systems Far from Equilibrium. Springer-Verlag, New York, NY, 1988, pp. 399-412.

28. Weigl, J., Baumeister, M., Influencing Factors and Their Effect on Coating Morphology, Deut. Papierwirt 3:147-162 (1980).

29. Hyman, W. A., Rheology of Power Law Fluids. I & EC Fund. 15:215-221(Aug. 1976).

30. Wesfreid, J. E.; Zaleski, S. Cellular Structures in Instabilities. Springer-Verlag, New York, 1984, pp. 1-19.

31. Guzy, C. J., Higgins, B. G., Viscous Pressure Across the Nip of a Blade Coater and its Effect on the Final Coated Film Thickness. Coating Conference Proceedings. TAPPI Press, Atlanta, GA. 1982:63-71.

32. Higgins, B. G., Dynamics of Coating, Adhesion and Wetting. Status Report, Project 3328, PAC Meeting, Appleton, WI, The Institute of Paper Chemistry, Mar. 24, 1981, pp. 69-74.

33. Li, A., Personal Communication, Rockton Research Center, Beloit Corp., Sept. 1989.

34. Gane, P.A.C., Coggon, L., Coating Blade Geometry: Its Effect on Coating Color Dynamics and Coated Sheet Properties. Tappi :87-96(Dec. 1987).

35. Pan, F., and Acrivos, A. Steady Flows in Rectangular Cavities J. Fluid Mech. 28: 643, (1967).

36. Bozeman, J.D., and Dalton, C. Numerical Study of Viscous Flow in a Cavity. J. Comp. Physics, 12: 348(1973).

37. Nallasamy, M., and Prasad, K, On the Cavity Flow at High Reynolds Numbers. J. Fluid Mech., 79: 391(1977).

38. Seydel, R., Practical Bifurcation and Stability Analysis, Elsevier Science Publishing, 1988.

39. Aidun, C.K. Stability of Convection Rolls in Porous Media. Bifurcation Phenomena in Thermal Processes and Convection, AMD-Vol. 89, edited by H.H. Bau, L.A. Bertram, and S.A.Korpela, 1987.

40. Bödewadt, U.T. Die Drehströmung über festem Grund. ZAMM 20: 241(1940).

41. Schlichting, H. Boundary-Layer Theory. Seventh Edition, McGraw-Hill, 1979.

42. de Val Davis, G., Mallinson, G.D. An Evaluation of Upwind and Central Difference Approximations by a study of Recirculating Flow. Computers and Fluids 4: 29 (1976).

43. Serrin, J. On the Stability of Viscous Fluid Motions," Arch. Ration. Mech. Analysis. 3:1(1959).

44. Benjamin, T.B. Applications of Leray-Schauder Degree Theory to Problems of Hydrodynamic Stability," Math. Proc. Camb. Phil. Soc. 79:373(1976).

45. Parker, J.R. Instability and the Papermaking Process. Fundamentals of Papermaking, Transactions of the 9th Fundamental Research Symposium. (C. Baker, V. Punton, ed.) Mechanical Engineering Publications, Cambridge, England, 1989, pp. 1183-1207.